9

Omoniyi, B. A., D. A. V. Stow, and A. R. Gardiner, 2018, Characterization of thin-bedded turbidites in the North Brae field, South Viking Graben, North Sea, *in* C. C. Turner and B. T. Cronin, eds., Rift-related coarse-grained submarine fan reservoirs; the Brae Play, South Viking Graben, North Sea: AAPG Memoir 115, p. 257–282.

Characterization of Thin-Bedded Turbidites in the North Brae Field, South Viking Graben, North Sea

Bayonle A. Omoniyi, Dorrik A. V. Stow,* and Andy R. Gardiner

Institute of Petroleum Engineering, Heriot-Watt University, Edinburgh EH14 4AS, Scotland, U.K. (e-mails: bayonle.omoniyi@gmail.com; D.Stow@hw.ac.uk; Andy.Gardiner@hw.ac.uk).

ABSTRACT

Heterogeneity in hydrocarbon reservoirs has significant impact on fluid flow during production and may lead to oil being trapped in low-permeability reservoir compartments. This is particularly true for producing turbidite fields with significant thin-bedded turbidite (TBT; 3–10 cm [1.2–3.9 in.] sand and silt unit) and very thin-bedded turbidite (VTBT; 1–3 cm [0.4–1.2 in.] sand and silt unit) successions. The principal geological attributes used to characterize TBT–VTBT include facies and facies associations, sandstone/mudstone ratio, bed geometry, sand connectivity, sediment texture, sedimentary structures, and vertical sequences of bed thickness. Their combination enables definition of four fundamental attribute indices that reflect the reservoir quality of TBT–VTBT successions. The attribute indices are sand connectivity index, sediment textural index, facies ratio index, and facies net-to-gross index.

Twenty TBT and VTBT facies are recognized in cores from North Brae field wells. The combination of results from the application of the attribute indices approach to core data from the field reveals six facies associations (FA), which may also be applicable elsewhere, each characterized by different attribute indices. FA1 has high-to-very-high sand connectivity and textural indices (mature, fine-medium-grained, well-sorted sand). Its core-based porosities and horizontal and vertical permeabilities indicate that it possesses the most favorable reservoir properties. For FA2, a lower sand connectivity index because of extensive mudstone lamination signals poorer quality reservoir features. FA3 and FA4 show moderate attribute indices and mixed reservoir quality facies, whereas more studies are needed to determine the suitability of FA5 and FA6 for potential shale gas exploitation in other areas.

*contact author

DOI:10.1306/13652184M1153811

INTRODUCTION

The Neglected Potential

This chapter contends that thin-bedded turbidites (TBTs) present a neglected potential within deep-water turbidite exploration and production. They have huge significance as both principal and marginal reservoirs, and for optimizing values of existing reservoirs, particularly in deep-water systems where investments are high and challenges severe. They have further significance as deep-water source rocks, as potential unconventional reservoirs, and, in the case of very thin-bedded turbidites (VTBTs), even as reservoir seals.

A large proportion of the world's major hydrocarbon reservoirs occur in deep-water turbidite systems (Pettingill, 1998; Stow, 2000; Stow and Mayall, 2000; Khain and Polyakova, 2004; Gluyas and Garrett, 2005; Hurst et al., 2005). Exploration in deep-water is increasingly active, with more than 50% of new discoveries in the past 10 years coming from deep-water plays. In the enterprise of growing reserves and optimizing field value in producing and marginal turbidite fields, the significance of TBTs (3–10 cm [1.2–3.9 in.] thick sand and silt unit) and VTBTs (1–3 cm [0.4–1.2 in.] thick sand and silt unit) cannot be overemphasized.

TBT and VTBT are volumetrically the dominant facies in deep-water systems, occurring throughout the spectrum of architectural elements in deep-water environments (Stow et al., 1996; Stow, 2000; Stow and Mayall, 2000). They occur both separately and in association with thick (30–100 cm [12–39 in.]) and very thick-bedded turbidites (over 100 cm [39 in.]), in which the latter form the most prolific deep-water reservoirs. Although they are not the best-quality hydrocarbon reservoirs, TBT–VTBT successions can significantly enhance hydrocarbon reserves in fields producing from deep-water sandstones (Shepherd, 1991; Clemenceau, 1995; Lerch et al., 1996; Clemenceau et al., 2000; Browne and Slatt, 2002). This is particularly true if their specific properties, such as porosity, permeability, and lateral and vertical connectivities, are correctly estimated and incorporated into the modeling of fluid flow and estimation of hydrocarbon recovery factor.

A classic example is the Paleocene Forties field (North Sea UKCS), which despite increased estimated ultimate recovery from 40% in 1972 to more than 65% in 2005 (Gluyas and Garrett, 2005) still has significant reserves left in the TBT and VTBT successions. These low-pay sands have now become primary targets for enhanced oil recovery in the Forties field and might be considered for development in other mature turbidite fields in the North Sea (e.g., fields described by Garland, 1993; Newton and Flanagan, 1993; Richards et al., 1993; Brehm, 2003; Fletcher, 2003; Wright, 2003; Hempton et al., 2005; Gill and Shepherd, 2010; Worthington, 2010).

This chapter applies a new quantitative approach developed for characterization of TBTs and VTBTs (Stow et al., 2012; Omoniyi et al., 2014, 2015) in the North Brae field, South Viking Graben, North Sea. The approach uses principal geological attributes that permit discrimination of TBT and VTBT facies in a variety of deep-water architectural elements. Combination of the attributes enables derivation of four attribute indices that provide quantification to TBT and VTBT properties such as lateral and vertical connectivities, sediment texture, and sand quality in the context of their depositional setting. The end results of the quantitative characterization may serve as both input parameters in running predictive simulation models or conditioning such models for economic recovery of hydrocarbon fluids bypassed in TBT and VTBT successions for overall field value optimization.

Previous Work

The present study focuses on North Brae field, which is one of a cluster of fields located at the western margin of the South Viking Graben as part of the Upper Jurassic play in U.K. Blocks 16/07 and 16/08 (Figure 1). The field, the first gas condensate recycling field to be developed in the North Sea, has an area of 19 km^2 (~7 mi^2), reservoir thickness in excess of 700 m (2300 ft), and average net to gross of 0.85. Its hydrocarbon column is 169 m (554 ft) thick with estimated recoverable reserves of 207 million bbl of condensate and 800 bcf of dry gas in its three-way dip closure. Production began in 1988 using a gas recycling mechanism to maintain reservoir pressure. The gas recovery factor is 80% (Stephenson, 1991; Brehm, 2003).

The Upper Jurassic Brae system was originally interpreted as a series of subaerial fan-deltas fringing marine sediments (Harms et al., 1981). This was then reinterpreted as a deep-water turbidite system of overlapping slope-apron fans, in which conglomerate and sandstone turbidites and debrites interdigitated with extensive TBT and VTBT facies (Stow et al., 1982; Stow, 1984). Turner et al. (1987) later referred to this as a multiple-source ramp. The different parts of this multiple-source ramp or slope-apron fans system show slightly different geometries, in which the North Brae field is dominated by a coarse-grained channel complex system (Stephenson, 1991), the Central Brae field by an unchanneled cone of coarse-grained sediment (Turner and Allen, 1991), and the South Brae field

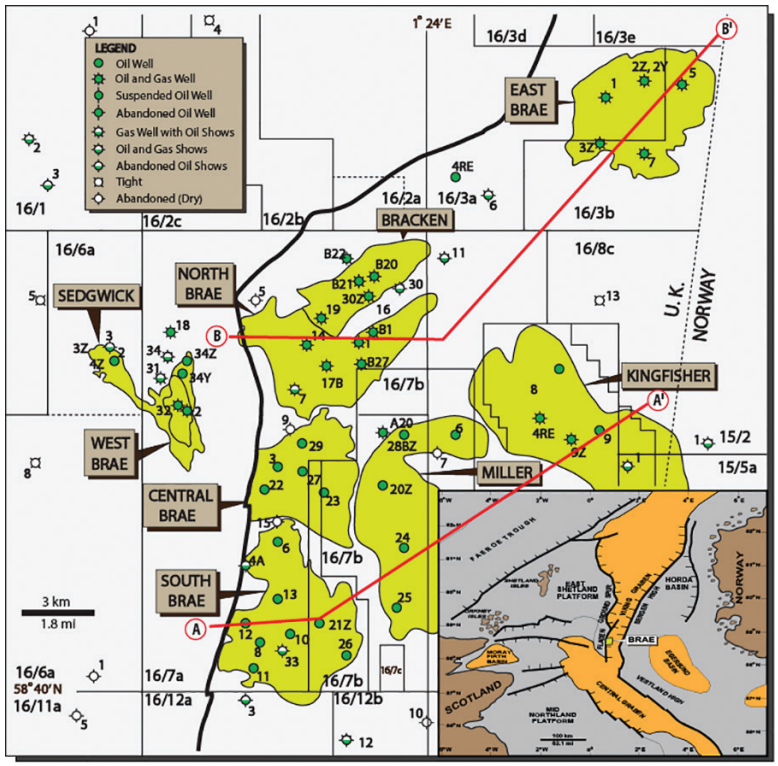

Figure 1. Map showing the location of the North Brae field (based on Brehm, 2003, figure 1), which forms one of a cluster of Upper Jurassic fields located at the western boundary of the South Viking Graben. Central Brae and South Brae lie to the south, Miller and Kingfisher to the east, and East Brae to the northeast. West Brae and Sedgwick fields have Eocene reservoirs. Two red lines show directions of cross sections along lines A–A^1 and B–B^1 in Figure 2.

comprises a radiating pattern of channel complexes (Roberts, 1991). The Bracken reservoirs (see Figure 1) are a northern arm of the channelized North Brae fan system, which partially overlies the Beinn field, a gas condensate accumulation within the Callovian Hugin Formation (Turner et al., 1987; Brehm, 2003; Fraser et al., 2003). There are several other influx points and sediment bodies recognized along the margin, not all of which result in good hydrocarbon reservoirs (Fraser et al., 2003).

According to Stow et al. (1982), the provenance for the Brae system sediments is the Fladen Ground Spur to the west, where a series of Devonian and older sediments and granites were uplifted as part of ongoing tectonic activity related to the Cimmerian orogenic episode. Alluvial fans and high-energy rivers fed sediment either onto a narrow shelf or directly onto a steep fault-controlled slope. Piano-key tectonics (Stow et al., 1983), in which different segments of the margin undergo tectonic uplift and subsidence at different times, has led to variation in the timing and amount of sediment input along the margin. East–west trending faults were probably important in separating the different parts (piano keys) of movement and in controlling the location of longer lived channels that served as conduits for sediment further eastward into the basin. Certainly, several discrete input points can be identified and linked to the short-headed channelized submarine fans that represent South, Central, and North Brae systems. Note that these are relatively small-scale systems that extend only about 20–25 km (~12–16 mi) from the fault margin into the basin. Schematic cross sections from margin to basin are shown in Figure 2.

The principal east–west-trending channel-fill complex of the North Brae field comprises sand-matrix conglomerates and sandstones flanked by TBT and VTBT slope facies (Brehm, 2003; Fraser et al., 2003; Turner et al., 2018). The conglomeratic facies pass eastward into predominantly sandstone facies and a sequence of sandstone–mudstone interbeds of the TBT and VTBT facies (Stow et al., 1982; Turner et al., 2018). Sandstone turbidites derived from the Fladen Ground Spur and fed via the South, North, and Central Brae complex channels form the principal reservoir facies of the Miller, Kingfisher, and East Brae fields that are located basinward (Rooksby, 1991; Garland, 1993; Branter, 2003; Spence and Kreutz, 2003). The thicker sandstone turbidites of these fields are interbedded with and pass laterally into TBT and VTBT facies. Garland (1993) described the thicker sandstones as interchannel deposits within a mid-fan setting. We consider them as terminal and interchannel sandy lobes.

Stratigraphically, the reservoir facies of all these fields (except Beinn) are part of the Upper Jurassic

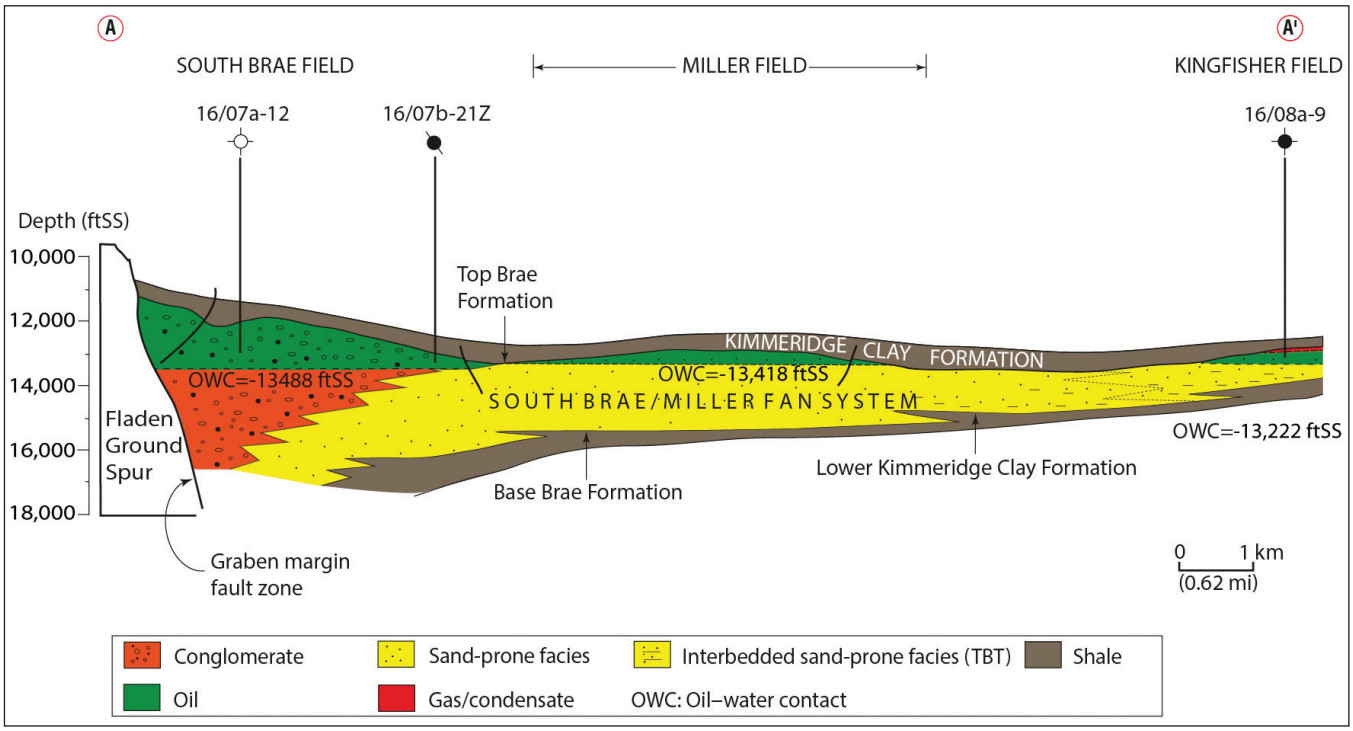

(A)

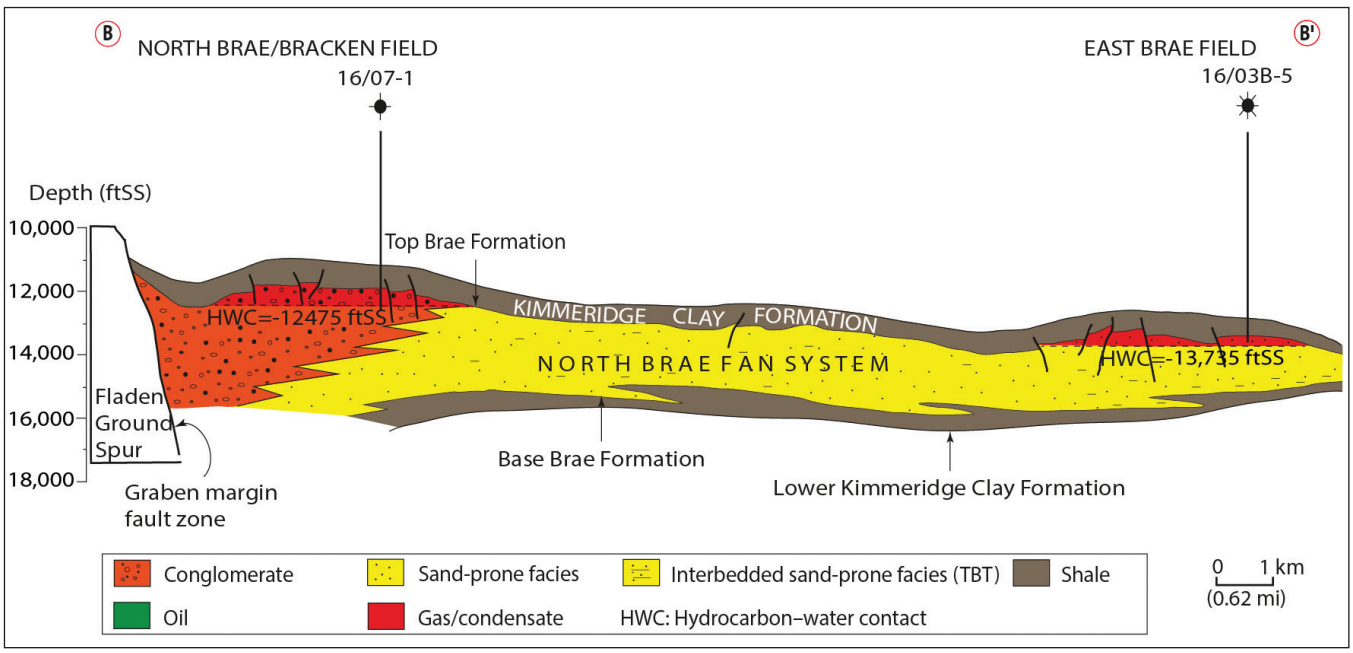

(B)

Figure 2. Schematic cross sections from margin to basin along lines A and B in Figure 1, illustrating the geometry of (A) the South Brae–Miller–Kingfisher submarine fan system, and (B) the North Brae submarine fan system, which probably extends north-easterly to East Brae. See text for explanation.

Brae Formation, which interdigitates with and is overlain by the Kimmeridge Clay Formation and is underlain by the Heather Formation (Figure 3). The Kimmeridge Clay Formation serves as both the top and lateral seal for the Brae reservoirs. These three formations, together with the Birch and Ling sandstone members, constitute the Humber Group (Turner et al., 1987).

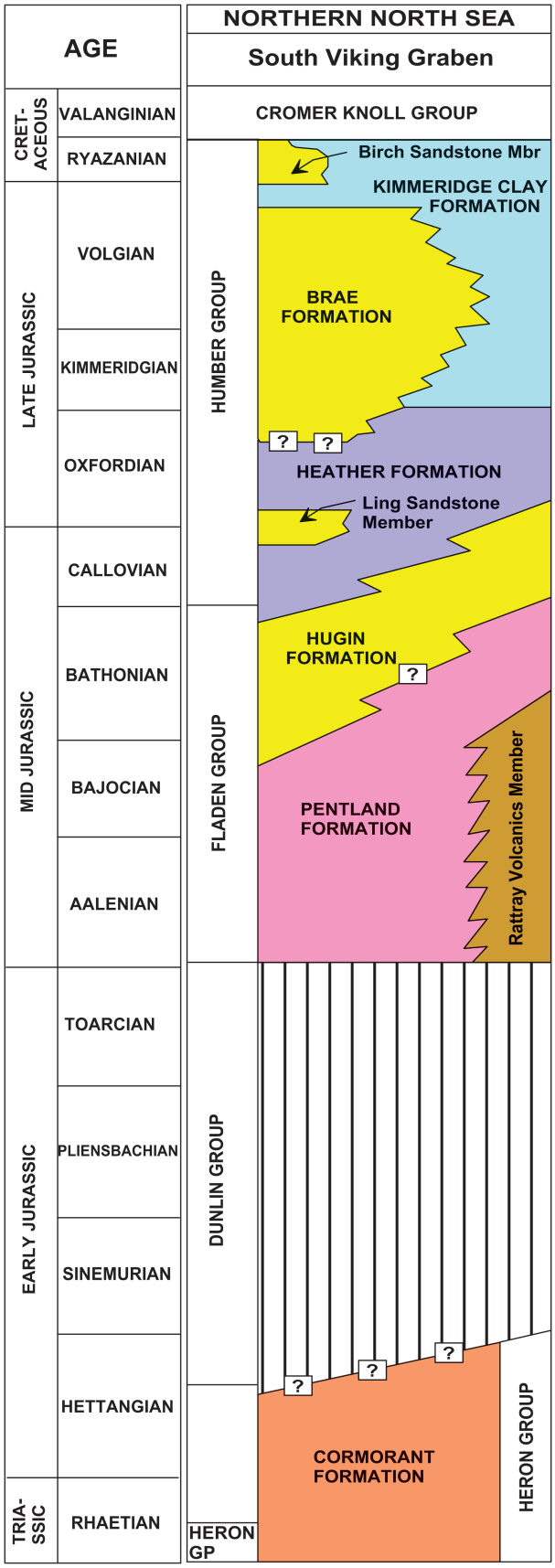

Figure 3. Lithostratigraphic chart of the South Viking Graben, Northern North Sea. The Upper Jurassic Brae Formation is part of the Humber Group and overlies the Heather Formation. It is overlain by and interdigitates with the Kimmeridge Clay Formation (modified from Turner et al., 1987).

METHODOLOGY

Wells and Wireline Logs

Nine wells from the North Brae field (Figure 4) have been examined for this study, principally using wireline log and core data. Cored intervals from four of these wells, comprising 98–100% TBT and VTBT facies, were selected for more detailed examination. Logging of over 1500 m (4921 ft) of core was carried out at 1:20 scale, and a total of 337.4 m (1107 ft) of the core was logged at 1:10 scale for a more detailed study. Core intervals logged are well preserved. The four wells selected for detailed study are 16/7a-7, 16/7a-B27, 16/7a-B14, and 16/7a-19 (Figure 4).

Gamma ray logs were used to delineate gross lithology. A combination of neutron and density logs enabled accurate lithology delineation and an estimate of the degree of shaliness. Based on the fact that sediment textural characteristics differ from one sediment type to another, boundaries between TBT successions and other facies were accurately delineated using sonic logs. In a typical TBT interval, sonic velocities become slightly higher (lower sonic transit times) because of the heterogeneous nature of the interval. Simple lithology logs were combined with the aforementioned wireline logs to permit accurate lithostratigraphic correlation and delineation of reservoir layers, using the top of Brae Formation as a datum. Well spacing was obtained from the top structure map of the study area.

Sediment Attributes and Attribute Indices

Drawing from a large number of studies of modern, ancient, and subsurface systems, we identify seven principal geological attributes of TBT and VTBT that can be used to discriminate between distinct facies and different architectural elements in deep-water systems. These geological attributes are facies and facies associations (FAs), sandstone/mudstone ratio, sandstone and mudstone geometry and dimensions, sand connectivity, sediment texture, small-scale sedimentary structures, and small-scale vertical sequences of bed thickness.

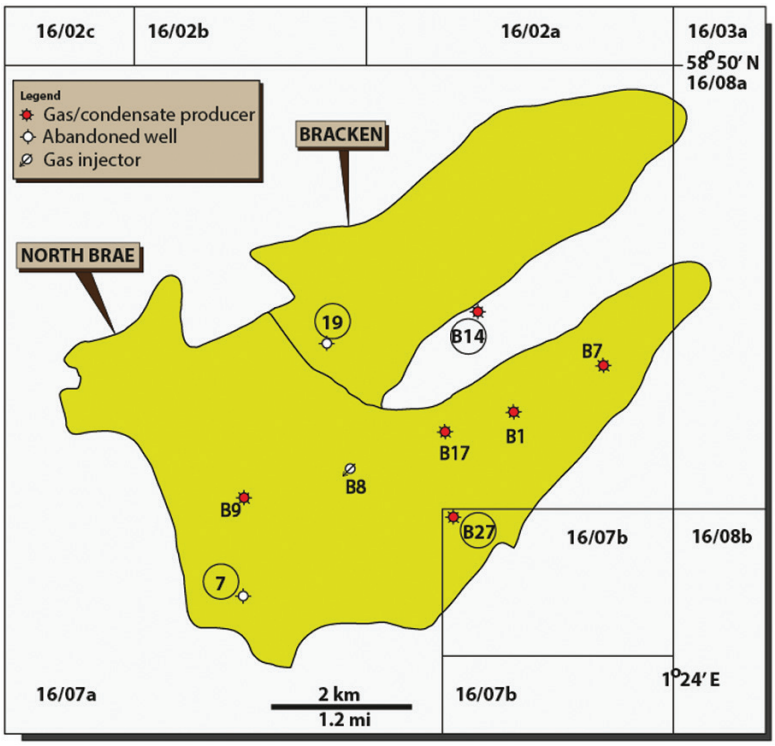

Figure 4. Outline of the North Brae field, including the Bracken reservoirs (Brehm, 2003), showing the wells used in the study. Circled wells were studied in detail.

Combination of these attributes enables definition of four principal attribute indices as follows:

1. Facies net-to-gross index (NGI)
2. Sand connectivity index (SCI)
3. Facies ratio index (FRI)
4. Sediment textural index (STI)

These indices provide numerical quantification of TBT and VTBT properties for input into reservoir simulation models. Further description of these attribute indices is given under the "Results" section in this chapter.

Bed Thickness Definitions

We use the definition of bed thickness as the thickness of a sediment unit that appears to have been deposited under essentially constant physical conditions (Selley, 2000). For turbidites, this generally includes the whole graded bed (i.e., both sand and mud parts of a graded bed). However, for the dual purposes of unambiguous measurement and applicability to reservoir characterization, we measure the thickness of the sand (or silt) part of the turbidite only. As the conventional definition of thin-bedded is 3–10 cm (1.2–3.9 in.) and of very thin-bedded is 1–3 cm (0.4–1.2 in.) (Stow, 2005), we therefore apply these thickness criteria to the sand (or silt) units. These definitions and practices are shown in Figure 5.

The bed thickness data acquired were plotted as bar graphs with depth (m or ft) on the vertical axis and bed thickness (cm) on the horizontal axis (Figure 6). A total of over 3000 beds have been measured and the basic statistics of bed thickness data derived from these data are the mean and standard deviation.

Porosity and Permeability

Forty-eight cylindrical core plugs were acquired from well B27 using an Eibenstock EBM 250/2P coring drill (25.25 mm [1 in.] diameter). Coring was carried out at discrete points to represent the FAs identified. Samples were subsequently trimmed at both ends, using a Cutrock GSP 1463 trimming saw. They were left to dry naturally for 6 days after which a digital Vernier caliper was used to accurately measure their dimensions. For each dimension, three readings were obtained and an average value was calculated and recorded.

A helium gas expansion Porosimeter MK II was subsequently used to measure sample porosity. This is capable of porosity measurements over a range of different sizes without instrument modification and also affords easy calibration. An EPS Nitrogen Gas Permeameter was used to measure permeability using backpressure flow technique. This technique enables accurate control of core pressure and flow rate while maintaining laminar flow rates in higher permeability samples.

RESULTS

North Brae Fan Architecture

Over 40 wells have been drilled into the North Brae fan system in the area of the North Brae field, many of which have been extensively cored and all of which have full sets of wireline logs available. Based on our own analysis of selected wells, as well as building on four previous publications (Stephenson, 1991; Turner and Allen, 1991; Turner and Connell, 1991; Brehm, 2003), we propose the following depositional architecture.

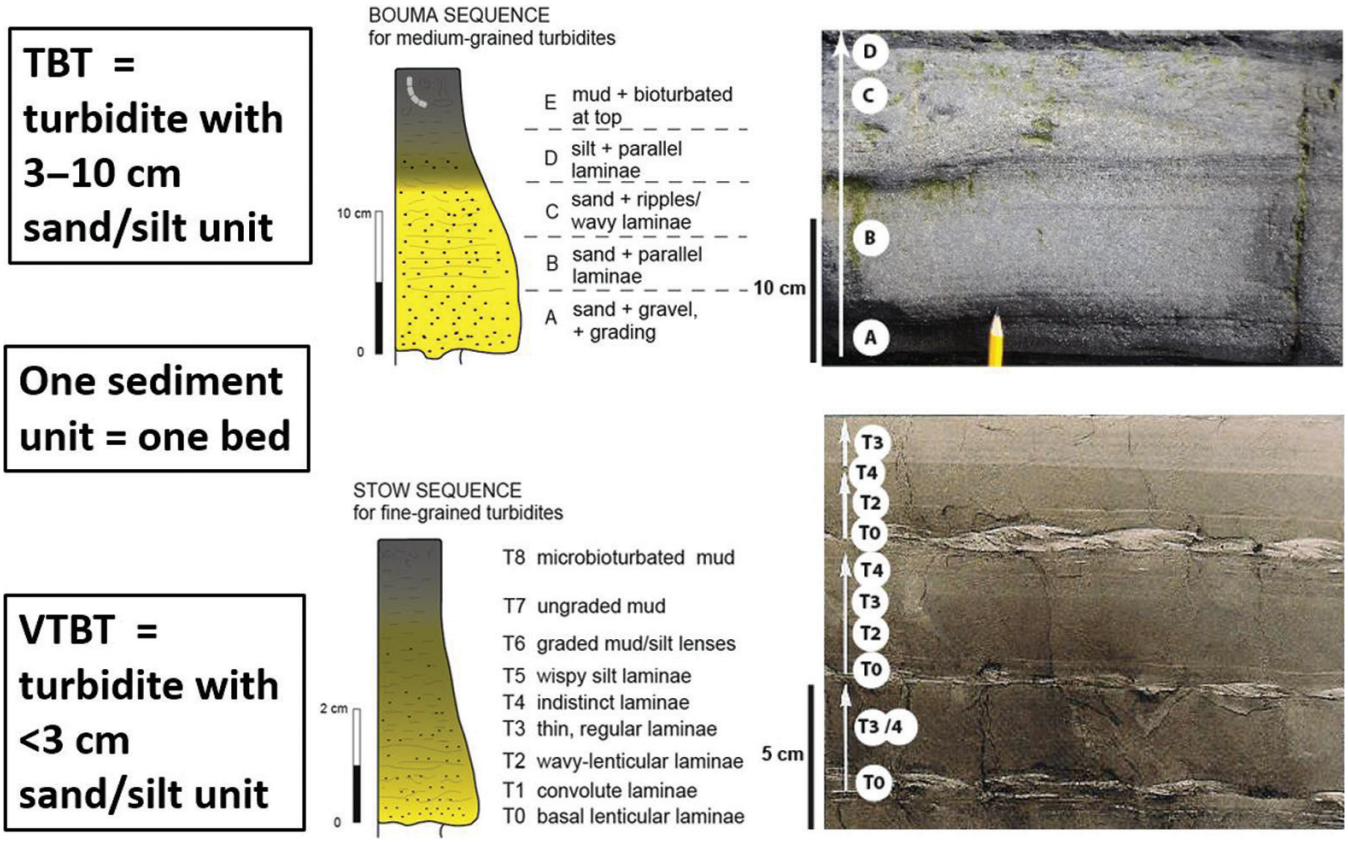

Figure 5. An illustrative definition of bed thickness as used in the study. A turbidite deposit comprising a 3–10 cm (1.2–3.9 in.) thick sand/silt unit is termed a thin-bedded turbidite (TBT). By contrast, a turbidite deposit with a sand/silt unit that is 1–3 cm (0.4–1.2 in.) thick is generally regarded as a very thin-bedded turbidite (VTBT). Where laminae (e.g., Stow's divisions) are present within a bed, they are treated not as disparate beds but as part of the bed (white arrows on the photos indicate individual TBTs or VTBTs).

The North Brae system is best referred to as a short-headed submarine fan linked to one specific input point along the faulted slope apron margin of the Late Jurassic. It extends eastward from this input point into the western part of the South Viking Graben and has a total radius of 15–20 km (~9–12 mi). The nature of sediment supply from the provenance region is uncertain, but the coarse-grained, poorly sorted nature of the facies suggests either an alluvial fan or high-energy fluvial system that delivered sediment directly to the principal feeder channel.

The fan radiates out from the input point (Figure 7), with one major conglomeratic channel system extending 5–8 km (~3–5 mi) basinward. The close tracking of principal fault lines to two of these channels suggests that their location may have been influenced by synsedimentary fault tectonics during Late Jurassic time. Sandstone-dominated facies (especially medium-bedded turbidites and TBTs) extend farther than 15 km (9 mi), reaching beyond the East Brae field (see Figure 2B); we interpret this area as mid-fan lobes. This region merges basinward into more mudstone-rich facies of the distal fan and basin plain. TBT and VTBT facies, although mostly absent from the channel-fill sections, occur in four distinct regions: (1) marginal to the input point and canyon, across a narrow slope-apron belt (e.g., wells 19 and 7); (2) adjacent to the northern channel, as a channel-margin facies (well B14); (3) across the mid-fan lobe region (well B27); and (4) in the distal fan to basinal area. It is the four wells referred to above that are examined further in this chapter.

Lithofacies correlation between individual wells has a high degree of uncertainty as the exact geometry and extent of individual conglomerate or sandstone bodies are not well constrained. Previous

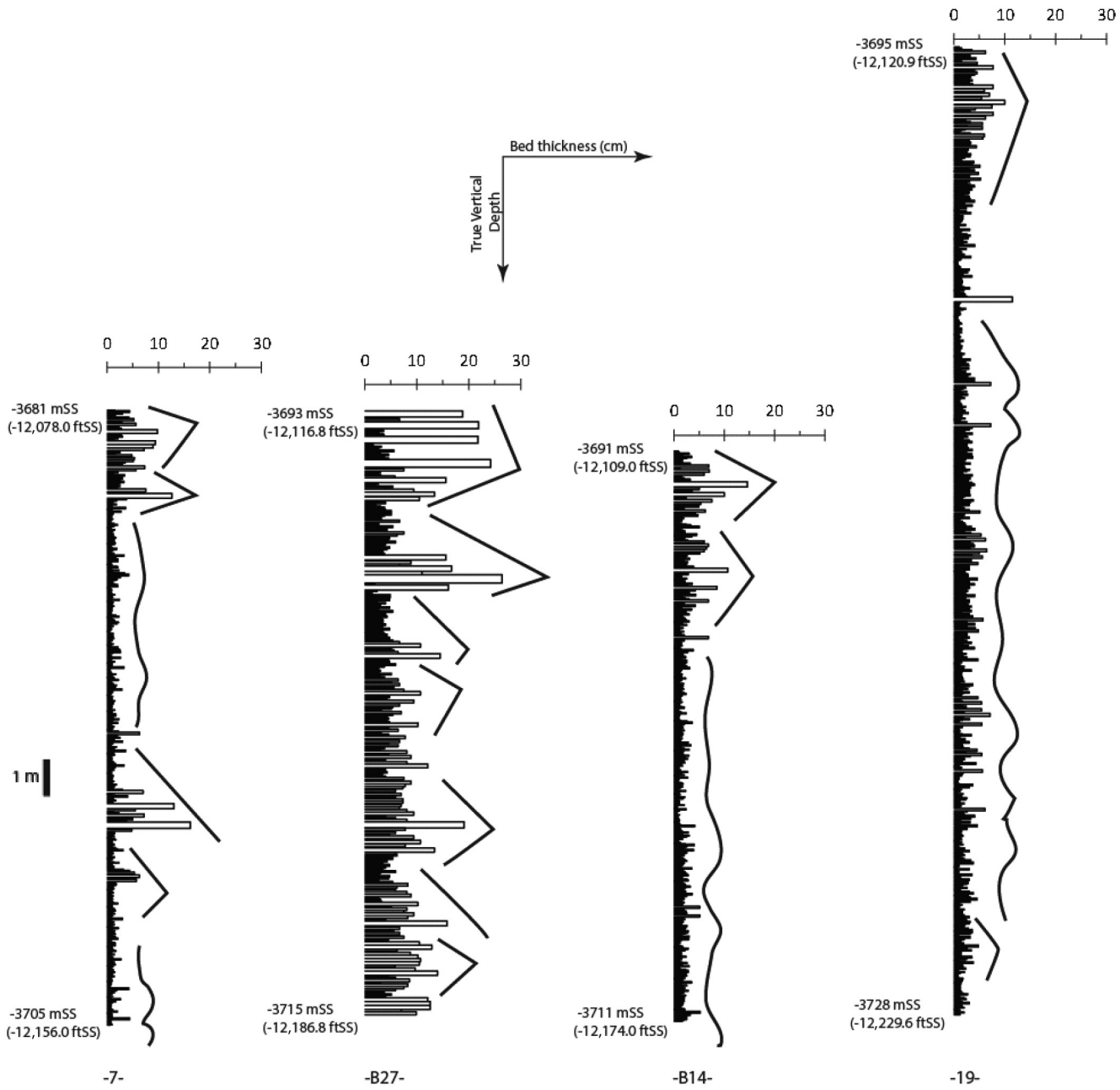

Figure 6. Bed thickness profiles for wells 7, B27, B14, and 19 for the intervals studied in detail within the cored intervals (see Figures 9A, 10A for core locations). The profiles reflect an irregular or oscillation sequence type (Stow et al., 1996) (e.g., B27), or a random noncyclic pattern (Piper and Stow, 1991) (e.g., 19). These are considered typical of slope apron, basin plain, and interchannel depositional environments.

studies have proposed lower and upper Brae reservoir units separated by a more or less widespread mudstone-rich layer (Stephenson, 1991; Brehm, 2003). These divisions are not everywhere apparent and are not easily applied to the wells examined for this study. Our down-channel (approximately east-west) cross section (Figure 8) shows the concentration of coarse-grained facies in what we interpret as the principal channels. These areas also represent the thickest depocenter for the upper Brae Formation, which reaches to over 350 m (1148 ft) thick. The two cross-channel cross sections (Figures 9, 10)

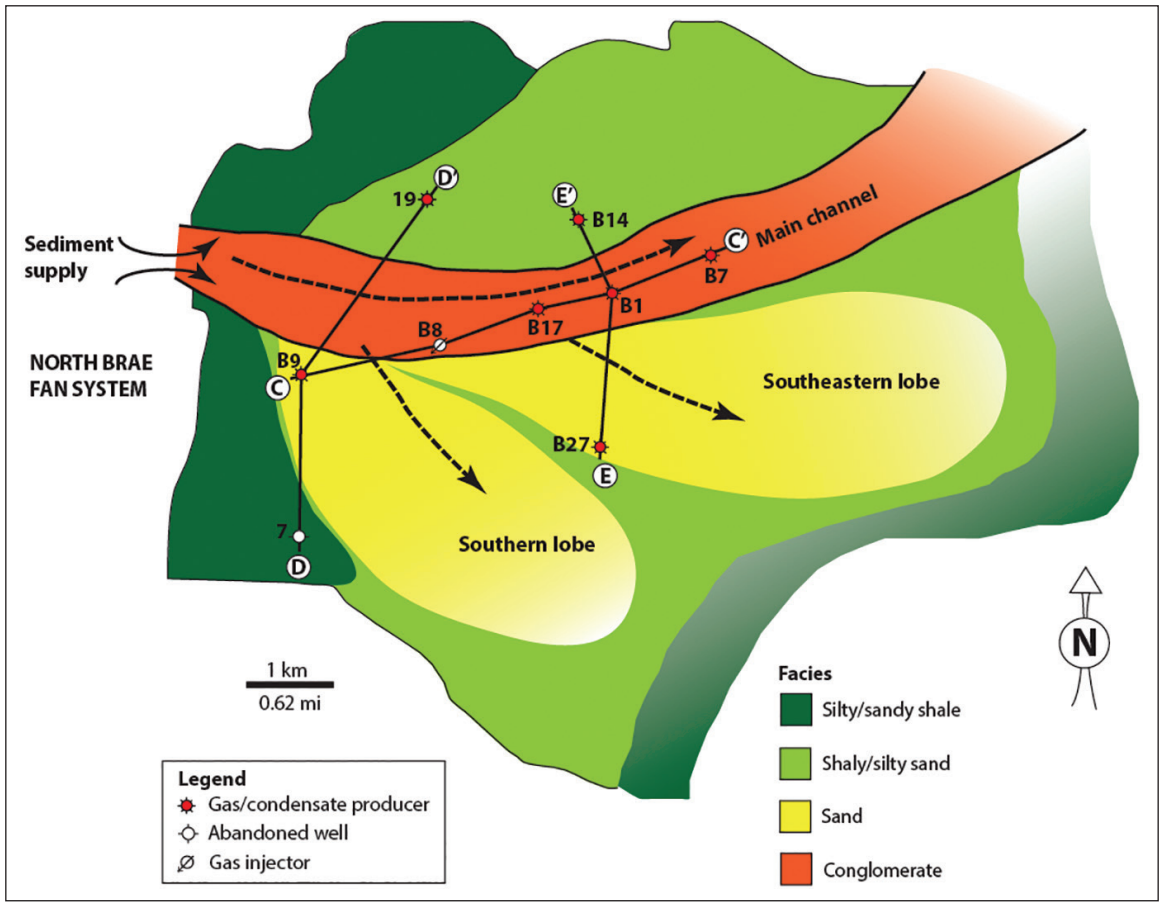

Figure 7. Facies distribution map for the upper part of the Brae Formation at the North Brae field. The black lines are correlation sections that are shown in Figures 8, 9, 10.

serve to illustrate the location and nature of the TBT and VTBT facies that both surround and interdigitate with the coarse-grained channel facies. These finer grained facies can be up to 270 m (885 ft) thick in places, with only very rare conglomerate intercalations.

Sediment Facies

Conglomerates, sandstones (medium- and thick-bedded turbidites), sandstones (TBT and VTBT), sandstone–mudstone units (TBT and VTBT), and mudstones (VTBT and hemipelagites) are the principal facies groups that occur in most of the wells examined (note that, for broad lithology terms used here, "sandstone" can in places include siltstone and "mudstone" comprises both clay- and silt-grade materials). In the four wells selected for detailed work, sandstone, sandstone–mudstone, and mudstone facies groups were further classified into 20 distinct facies on the basis of composition, grain size, type of bedding and lamination, internal structures, and average sandstone/mudstone ratio. Within these 20 distinct facies, we recognize 9 that are dominantly sandstone-rich, 5 that are mixed sandstone–mudstone, and 6 that are dominantly mudstone–siltstone. The full range of facies names are presented in Table 1 and in Figure 11 for the purpose of illustration. The facies are discussed briefly below.

S1: Structureless Planar-Bedded Sandstone Facies S1 occurs as an ungraded and largely structureless, well-sorted medium light gray fine- to medium-grained sandstone with mean grain diameter of 131.52 µm, mean sphericity of 0.36, and mean aspect ratio of 1.85. With the exception of rare mudstone drapes that tend to occur irregularly, the facies is composed entirely of sandstone.

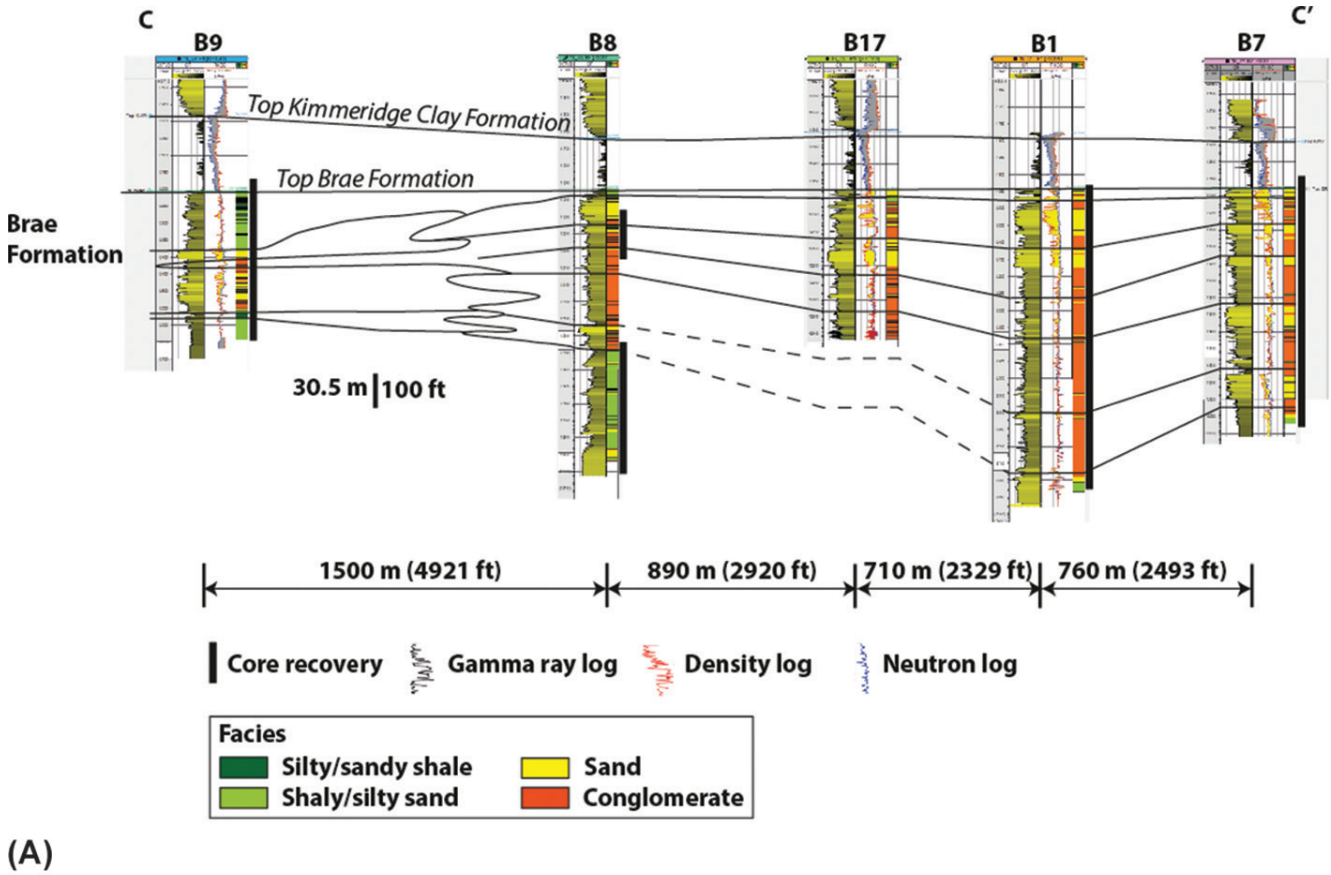

Figure 8. Stratigraphic framework (A) and lithostratigraphic units (B) based on careful correlation of a suite of wireline logs (gamma ray, density-neutron, and sonic) and core data, showing sediment stacking pattern along the main conduit, that is, central channel (line C–C^1). Core locations are shown as black thick lines (A). Numbers at the base are the distances between the wells. Well depths are in TVDSS, and wells are hung at the top of the Brae Formation.

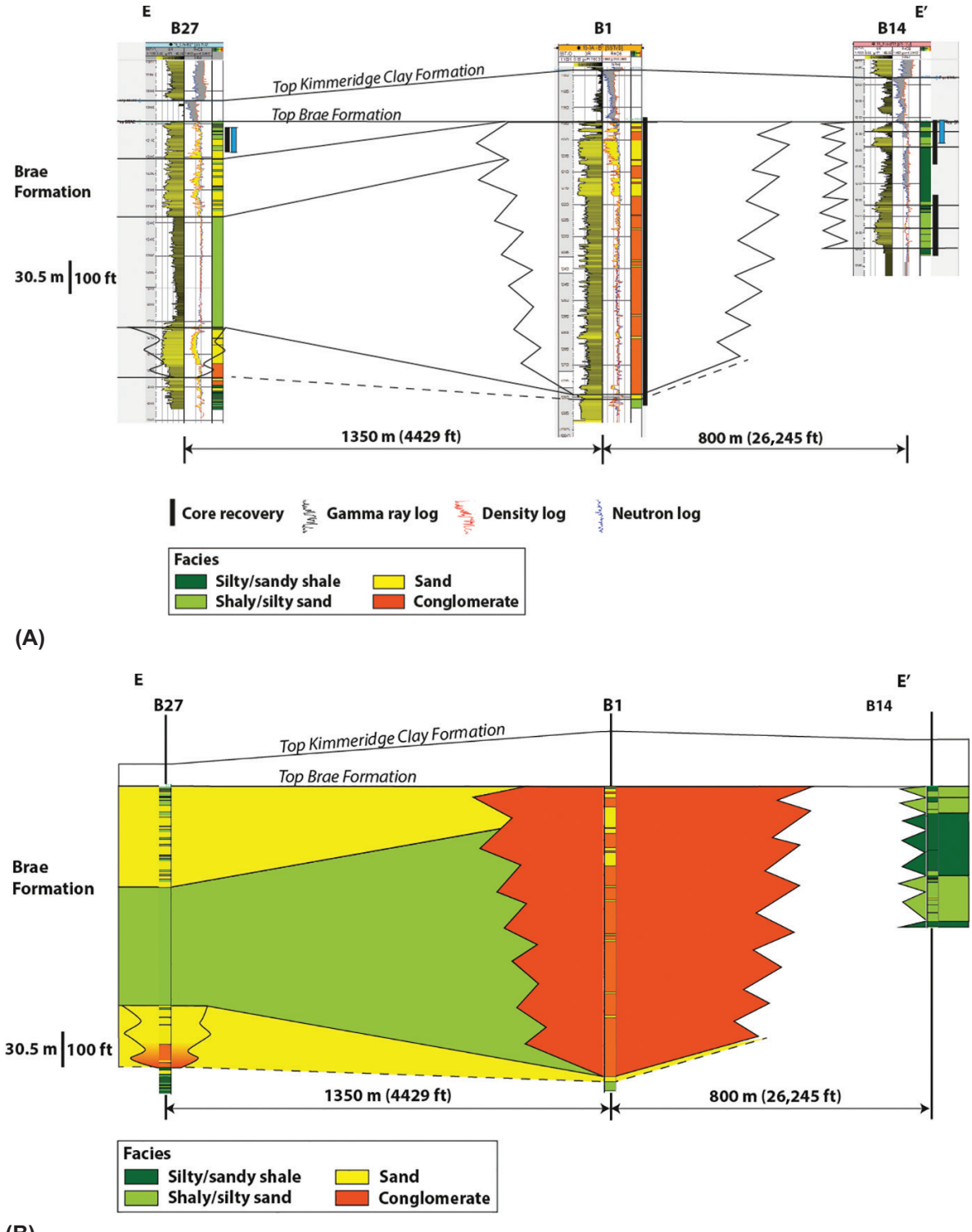

Figure 9. Stratigraphic framework (A) and lithostratigraphic units (B) based on careful correlation of a suite of wireline logs (gamma ray, density-neutron, and sonic) and core data, showing sediment stacking pattern, transverse to the principal sediment fairway (line E–E[1]). Core locations are shown as black thick lines, and the parts of cores shown in Figure 6 as blue lines (A). Numbers at the base are the distances between the wells. Well depths are in TVDSS, and wells are hung at the top of the Brae Formation.

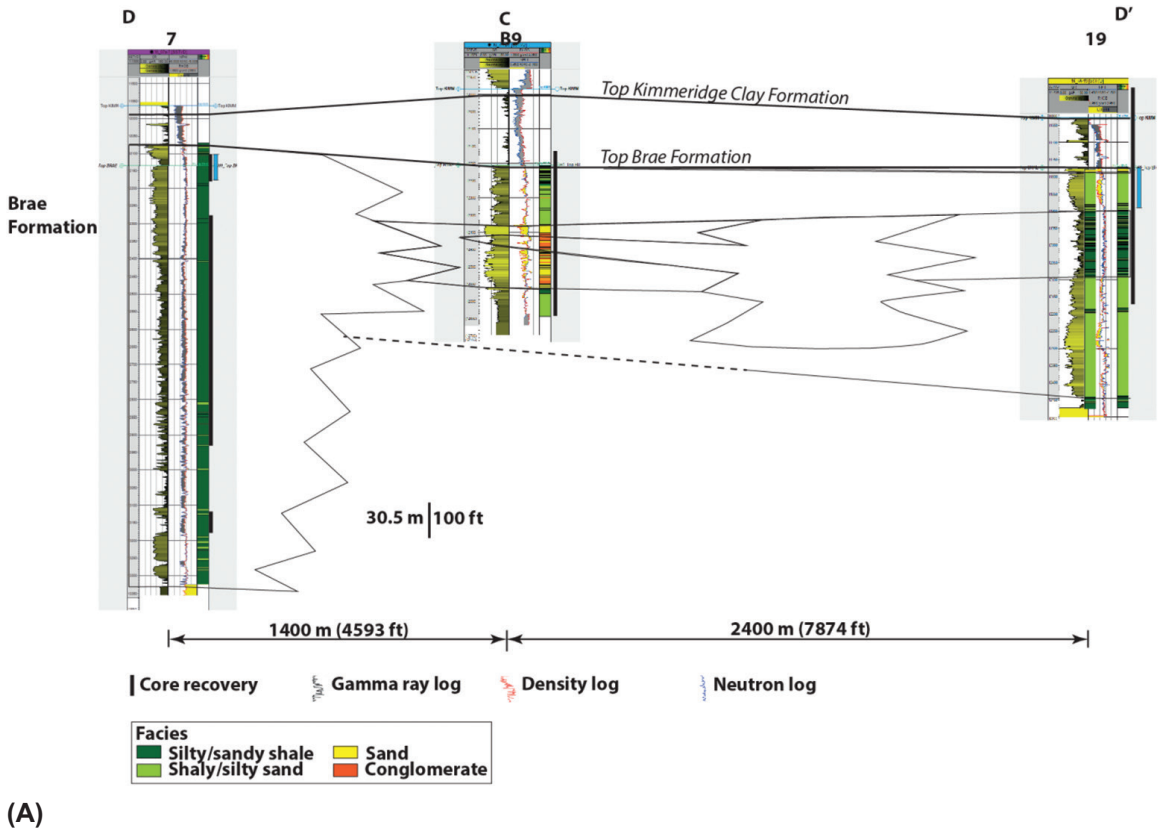

(A)

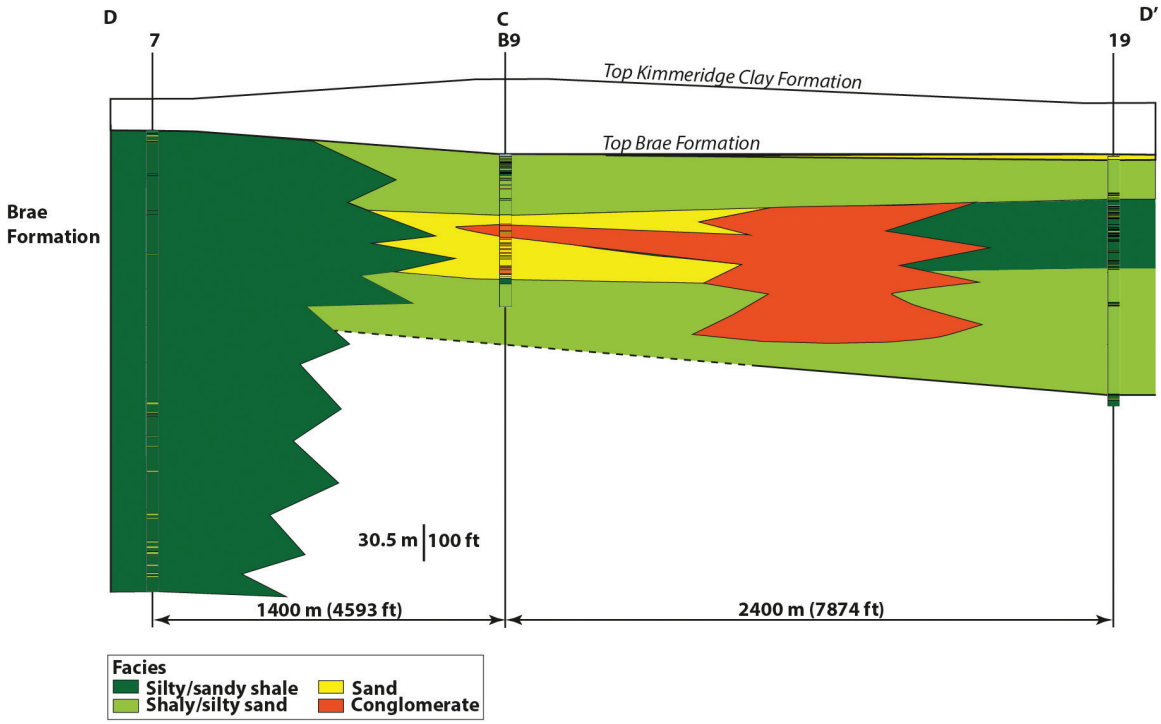

(B)

Figure 10. Stratigraphic framework (A) and lithostratigraphic units (B) based on careful correlation of a suite of wireline logs (gamma ray, density-neutron, and sonic) and core data, showing sediment stacking pattern, transverse to the principal sediment fairway (line D–C–D[1]). Core locations are shown as black thick lines, and the parts of cores shown in Figure 6 as blue lines (A). Numbers at the base are the distances between the wells. Well depths are in TVDSS, and wells are hung at the top of the Brae Formation.

Table 1. Proposed thin-bedded and very thin-bedded turbidites facies.

Class	Facies Code	Facies Name
Sandstone	S1	Structureless planar-bedded sandstone
	S2	Rippled planar-bedded sandstone
	S3	Crudely laminated sandstone
	S4	Rippled wavy-laminated sandstone
	S5	Planar interlaminated sandstone
	S6	Planar, parallel- to ripple-laminated sandstone
	S7	Flaser-bedded sandstone
	S8	Convolute-laminated sandstone
	S9	Disturbed silty sandstone with contorted lamination
Sandstone–mudstone	SMI	Mud-draped wavy/planar subparallel sandstone
	SM2	Sandstone–mudstone grade with disrupted lamination
	SM3	Planar-bedded muddy sandstone
	SM4	Interbedded sandstone with laminated mudstone
	SM5	Interlaminated sandstone with nonlaminated mudstone
Mudstone ± sandstone/siltstone	M1	Parallel interlaminated mudstone
	M2	Lenticular interlaminated mudstone
	M3	Chaotic mudstone
	M4	Graded mudstone
	M5	Ungraded mudstone with isolated flat lenses
	M6	Structureless mudstone

Within S1 beds, sandstone is separated by a very thin mud drape that makes up less than 1% of the sediment. Characteristic bed thickness ranges from 4.5 cm (~2 in.) to over 10 cm (~4 in.), but beds thicker than 15 cm (~6 in.) also rarely occur. The absence of scoured bases and distinct lamination suggests similarity to the upper unit of the Bouma A-division sandstone.

S2: Rippled Planar-Bedded Sandstone S2 facies are often interbedded with S4 and SM5, and individual sandstone beds are commonly separated by distinct very thin siltstone with mud lamina (M1). However, within successive S2 beds (2.2–8.5 cm [0.9–3.3 in.] thick), bedding is less distinct and is reflected by an abrupt change in color, from light olive gray to olive black beds. Like S1 sandstone, the facies has a very high sandstone/mudstone ratio, with sandstone content up to 98%, but differs in its characteristic sediment composition. It comprises moderately-to-well-sorted, very fine- to medium-grained sandstone with subtle internal grading that is displayed by textural changes from a lower dominantly fine- to medium-grained interval to an upper interval of very fine-grained sandstone. Both the dominant current-rippled and thin siltstone laminae that form the bed boundaries are indicative of Bouma C- and D-division sandstone.

S3: Crudely Laminated Sandstone With respect to bed thickness, color, and grain size, S1 and S3 are congruent facies. In other words, S3 differs only in the presence of faint planar-parallel lamination. S3 facies is less common within a TBT succession than the S1 facies and is generally overlain by M1, M4, or M5 facies. The faint but noticeable planar-parallel lamination, together with the overlying facies types, is typical of base-missing Bouma B- and D-divisions and Stow's T0/T1, T2-T3/T5 divisions.

S4: Rippled Wavy-Laminated Sandstone Facies S4 deposits are similar to the planar-bedded counterparts in S2 but with additional wavy lamination and a more uniform bed thickness that uncommonly exceeds 4 cm (1.6 in.). In addition, the facies has a marked darker color that reflects mud-lined wavy lamination under ultraviolet (UV) light, indicating a slightly lower sandstone/mudstone ratio. The current ripples, unlike those of the S2 deposits, are more prominent but confined within wavy nonparallel laminae.

S5: Planar Interlaminated Sandstone Beds within a unit of S5 facies have gradational contacts and respective bed boundaries are very difficult to identify.

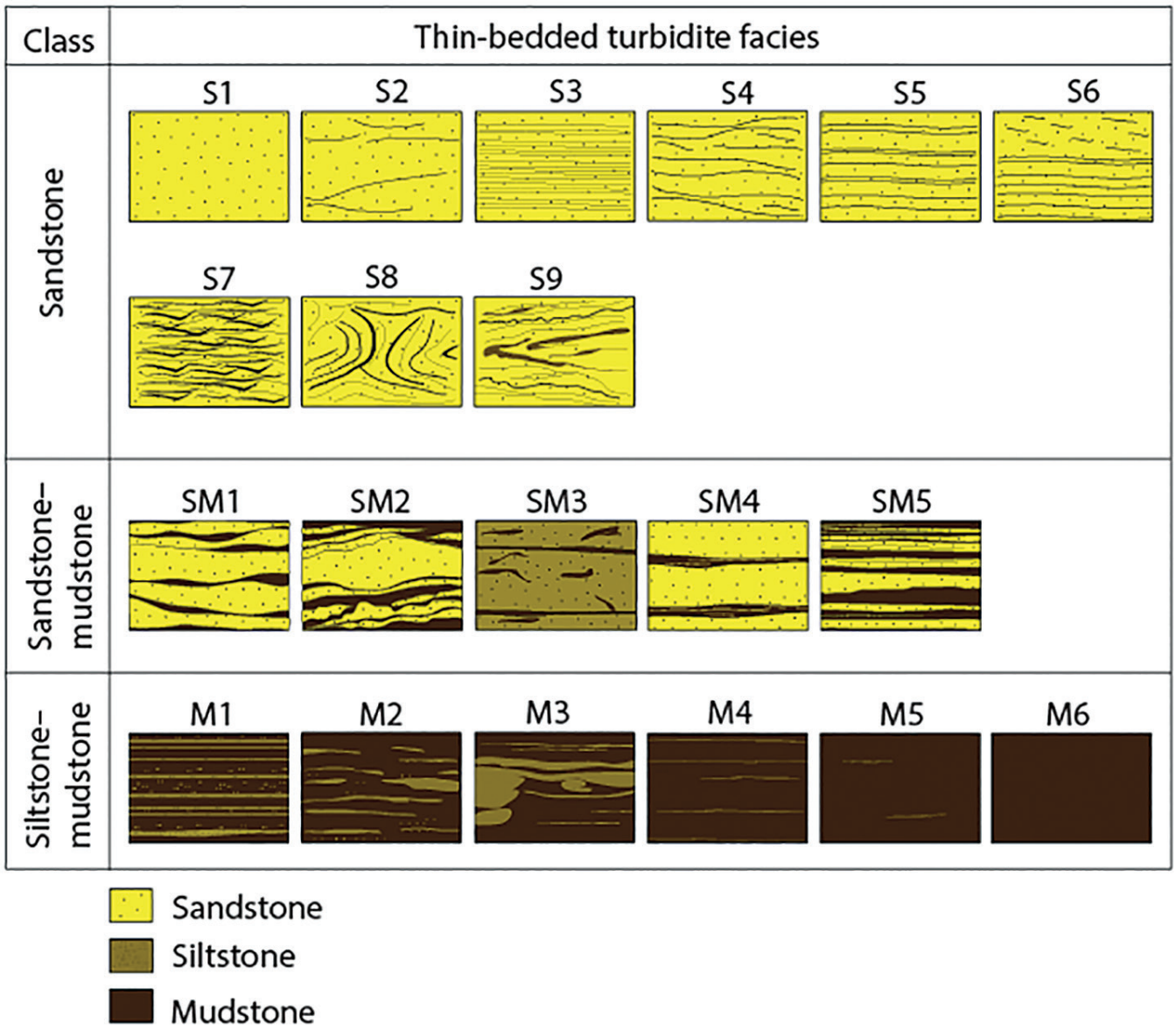

Figure 11. Illustration of thin-bedded and very thin-bedded turbidite lithofacies scheme based on their composition, grain size, bedding and lamination style, internal structures, and average sandstone/mudstone ratio. Within the 20 distinct facies, 9 are dominantly sandstone-rich, 5 are mixed sandstone–mudstone, and 6 are dominantly mudstone–siltstone.

However, adjacent to other facies, bed boundaries are sharp and planar. Individual beds, where sufficiently clear, may reach up to 3 cm (1.2 in.) in thickness. The facies has a sandstone/mudstone ratio that is higher than S4 facies but lower than for S1, S2, and S3 facies. Under UV light, there is a marked color change (dominantly very light gray) imprinted on it by calcite cementation, and internal grading toward the top can be clearly seen by the color change. The facies represents Bouma B- and lower C-divisions and is characterized by variable bed thickness.

S6: Planar, Parallel- to Ripple-Laminated Sandstone

S6 bears much resemblance to S5 facies with respect to grain size and sandstone/mudstone ratio. On the other hand, internal grading is more pronounced in the former than the latter, with a lower, planar-parallel, fine-grained sandstone grading upward to ripple-laminated very fine-grained sandstone. Bed boundaries between S6 and neighboring facies are sharp to gradational, and individual beds are within the range of 4–10 cm (1.6–3.9 in.) in thickness.

S7: Flaser-Bedded Sandstone The mud streaks confined within troughs of current ripples within S7 beds result in the darker greenish color that reflects a lower sandstone content than the preceding facies. Bed boundaries between successive beds of S7 facies cannot be easily identified because of its monotonous but complex internal organization across respective bed intervals. Toward the top of these intervals, grain-size gradation occurs and the top is commonly capped by M1 and rarely by SM5 facies. By estimation, bed thickness appears to exceed 10 cm (3.9 in.) in places.

S8: Convolute-Laminated Sandstone The convolute-laminated sandstone facies comprises fine-grained sandstone with deformed internal lamination. It has a lower sandstone/mudstone ratio than the preceding facies and lacks regular internal structure. Ripples are rarely seen and wavy laminations are poorly organized, causing an irregular pattern that reflects rapid settling of sediment from a dilute turbidity current. It is the least common facies in the core sections examined and, when present, it is over 12 cm (4.7 in.) in thickness. Characterized by planar bedding, the facies is separated from undeformed beds by sharp boundaries. Other than the deformed lamination, the facies closely resembles S1.

S9: Disturbed Silty Sandstone with Contorted Lamination Unlike S8 beds, relict internal laminations in S9 beds are well preserved. The latter have typically gradational boundaries and the facies has a lower sandstone/mudstone ratio. It is difficult to accurately measure individual bed thickness because of profound blurring of bed boundaries marked by a mix of various grain sizes. However, distinct boundaries can occur with other facies, where marked color changes and improved internal organization emphasize bed boundaries.

SM1: Mud-Draped Wavy/Planar Subparallel Sandstone This facies, like SM2, SM3, SM4, and SM5, comprises sandstone with variable proportion of mudstone. Typically, the mudstone forms thin drapes over sandstone beds that rarely exceed 3 cm (1.2 in.) in thickness. Unlike other members of the sandstone–mudstone class, one or two beds comprising S2 facies are usually sandwiched within its intervals. The average sandstone/mudstone ratio within individual beds is 5:1 and these beds are sharp-based and sharp-topped.

SM2: Sandstone–Mudstone Grade with Disrupted Lamination The presence of sharp bed bases and gradational tops, in addition to discontinuous wavy subparallel laminae of thin-to-medium thickness, differentiate SM2 from SM1 facies. The discontinuous laminae are often silty in SM2, in contrast to the continuous sandy wavy laminae of SM1. Bed thickness is commonly in the range of <1 to 5 cm (0.4–2 in.), and M1 and M4 are the most common associated facies.

SM3 (Planar-Bedded Muddy Sandstone) and SM4 (Interbedded Sandstone with Laminated Mudstone) Both SM3 and SM4 facies have similar textural and bedding characteristics. The former comprises a mixture of sandstone and mudstone, giving it a characteristic very light gray color and poor sorting, whereas the sandstone in the latter is both cleaner and better sorted. Individual sandstone beds that make up SM3 are up to 6 cm (2.4 in.) in thickness, contain mudstone clasts, and are marked by sharp, planar boundaries adjacent to mudstone laminae. By contrast, beds composed of SM4 are thinner, lack mudstone clasts, and have gradational boundaries.

SM5: Interlaminated Sandstone with Nonlaminated Mudstone This TBT facies is composed of alternating lighter (very fine-grained sandstone) and darker layers (nonlaminated mudstone). The couplets differ from those of the SM2 facies by being thinner (<1 to 2.6 cm [0.4–1 in.]) and internally graded (from very fine-grained sandstone to nonlaminated mudstone). Sharp bases and gradational tops separate individual beds from associated facies.

M1: Parallel Interlaminated Mudstone Very fine-grained sandstone and siltstone laminae give the mudstone of M1 facies a monotonously thin interlaminated character that distinguishes it from the sand-bearing SM5 facies. The M1 facies has a relatively low siltstone content of about 15% (average), with individual lamina having sharp bases and gradational tops.

M2: Lenticular Interlaminated Mudstone M2 facies is mudstone-dominated but comprises partially connected flat- to lens-shaped laminae of siltstone and very fine-grained sandstone that give it a characteristic lenticular lamination. Within individual siltstone and sandstone lenses, sorting is moderate and textural grading is subtle. The thicknesses of these lenses appear to reduce toward the top of a facies unit.

M3: Chaotic Mudstone As in the M2 facies, bed boundaries within the M3 facies are sharp-based and sharp-topped. The moderately sorted siltstone and very fine-grained sandstone laminae appear to have been loaded into the underlying graded mudstone, giving it a chaotic internal structure. The siltstone/mudstone ratio for the M3 facies is the highest among the siltstone–mudstone couplet facies.

M4: Graded Mudstone; M5: Ungraded Mudstone with Isolated Flat Lenses; M6: Structureless Mudstone M4 facies consists of crude, very thin to thin siltstone laminae aligned parallel within a background of mudstone. This repetition of siltstone laminae gives the mudstone a graded appearance. In some cases, however, only very few siltstone lenses (often flat and isolated) are present (M5), and these lenses may be completely absent as in the case of structureless mudstone (M6). These three facies are completely lacking in sand content and no significant siltstone content is adequate to permit measurements of bed thickness.

TBT and VTBT Facies Associations

For ease of comparison and analysis, the fine-grained facies have been grouped into six FAs using distinctive attributes such as sand percentage and internal structure (Figure 12). These are defined as follows:

FA1: average 90–95% sand, TBT and VTBT, beds mainly <5 cm (2 in.) thick, mudstone laminae and drapes only, mostly Facies S1–S9.

FA2: average 80–90% sand, TBT and VTBT, some beds up to 10 cm (~4 in.), some medium-bedded turbidites, mudstone layers more marked than FA1, mostly facies S1–S9, some facies SM1–5.

FA3: average 60–80% sand and silt, VTBT dominant, some TBT (<5 cm [2 in.]), mudstone laminae and drapes, mostly facies SM1–5, some facies S1–S9.

FA4: average 40–60% sand and silt, VTBT dominant, some TBT, mostly SM1–5.

FA5: average 20–40% sand and silt, VTBT dominant, rare TBT, mostly facies SM1–5 and M1–3.

FA6: average <20% silt and very fine sand, VTBT and mud only, mostly facies M1–6.

The proportions of these different FAs (Table 2) vary markedly between the cored intervals of the four wells (7, B27, B14, and 19) subjected to the detailed study (Figure 13). The most sand-rich facies (FA1–FA2) characterize the studied core from well B27 in the mid-fan lobe succession, and the lower half of

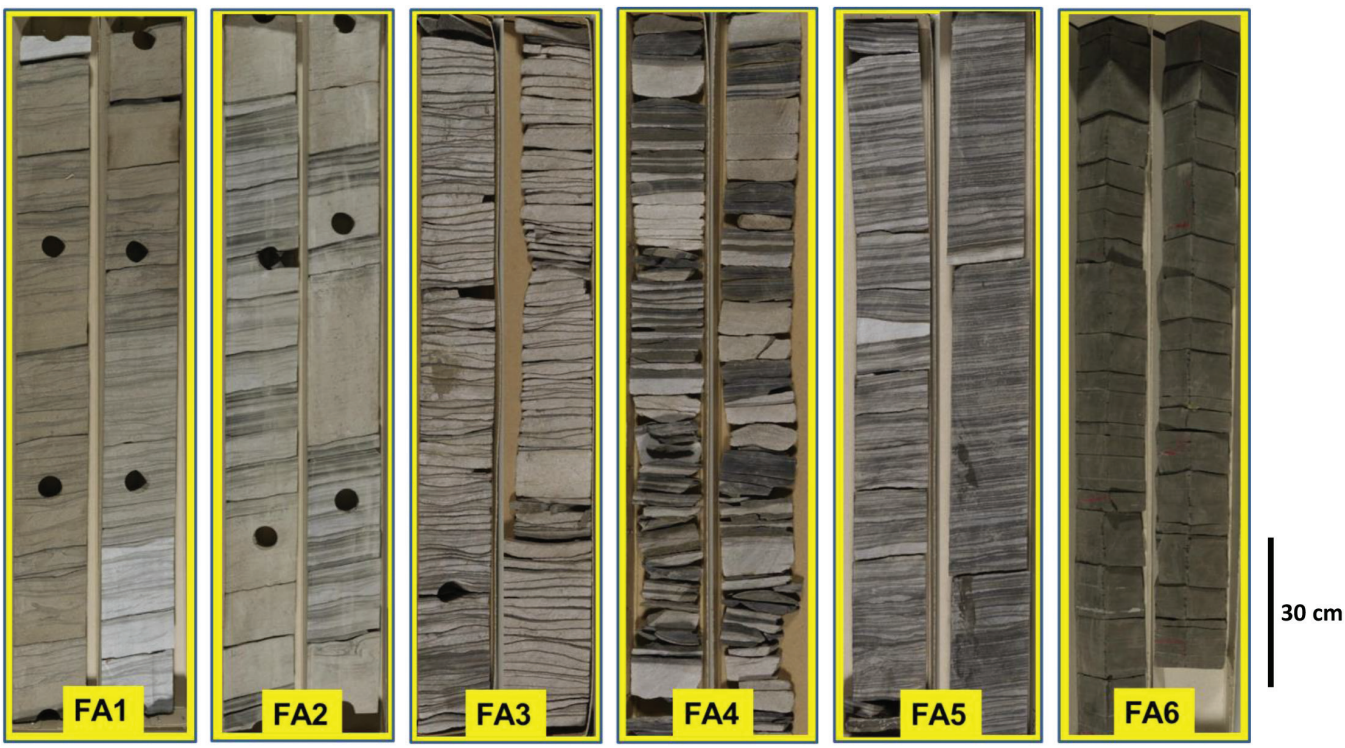

Figure 12. Core photographs of TBT and VTBT facies associations. Lithofacies identified were grouped into six associations based on their composition, sandstone/mudstone ratio, and nature and type of bedding.

Table 2. Proportion of facies associations in four wells in the North Brae field.

Facies Associations	Percentage Proportion of Facies Associations in Wells			
	7	B27	B14	19
1	0	59	0	67
2	0	35	0	0
3	42	0	43	0
4	58	6	32	13
5	0	0	25	20
6	0	0	0	0

the core from well 19. The more sand and mud-rich facies (FA4–FA5) are most common in the B14 core, the channel-margin succession, and in the upper parts of core from wells 7 and 19 in the slope-apron succession.

Bed Thickness and Sequences

Bed thickness data for wells 7, B27, B14, and 19 (Figure 6) are based on selected cored intervals from near the top of the Brae Formation of around 20 m (65 ft) in wells 7, B27, and B14, and 35 m (115 ft) in well 19 (see Figures 9, 10 for core locations). These profiles show no convincing vertical trends or sequences of bed thickness variation. Instead they all reflect an irregular or oscillation sequence type (Stow et al., 1996) or a random noncyclic pattern (Piper and Stow, 1991). These are considered typical of slope apron, basin plain, and interchannel depositional environments. Small-scale oscillation sequences, compensation cycles, or microcycles are quite possibly also present, especially in the mid-fan lobe succession of well B27 (Figure 14). Further work is needed to validate these trends.

Bed thickness statistics for the measured intervals in wells 7, B27, B14, and 19 (Figures 13, 14) are presented as frequency distribution curves (Figure 15A) and bar charts (Figure 15B). Three of the wells are closely comparable, each having excess of 90% VTBTs (Figure 15A). Core from well 7 consists of 97.6% VTBTs and 2.2% TBTs, with a mean bed thickness of 0.9 cm (0.35 in.) and standard deviation of 1.0 cm (0.39 in.). Core from well B14 comprises 95.3% and 4.6% of VTBTs and TBTs, respectively, with a mean bed thickness of 1.2 cm (0.47 in.) and standard deviation of 1.1 cm (0.4 in.). Core from well 19 consists of 90.3% and 9.8% of VTBTs and TBTs, respectively, with a mean bed thickness of 1.3 cm (0.5 in.) and standard deviation of 1.3 cm (0.5 in.). By contrast, well B27 core has 41.5% VTBTs and 51.6% TBTs, with a mean bed thickness of 4.9 cm (1.9 in.) and standard deviation of 3.6 cm (1.4 in.). In each well, a relatively small proportion of beds lie in the medium range of bed thickness (i.e., 10–30 cm [~4–12 in.]). This amounts to between 0.1% and 0.2% in wells 7, B14, and 19, but up to 6.9% of beds in well B27.

Attribute Indices

Understanding the dynamic behavior of reservoirs is critical to reducing key uncertainties and mitigating attendant subsurface risks that impact hydrocarbon recovery in VTBT and TBT reservoirs. To achieve this, we define a new quantitative approach to provide input parameters for reservoir simulation models that will predict flow of hydrocarbon fluids in such reservoirs. The four attribute indices used for this study are defined and explained below.

Facies Net-to-Gross Index (NGI) NGI is an index that expresses the standard net-to-gross sand value commonly used to evaluate reservoir intervals. We have made it more closely aligned with TBT and VTBT facies by calculating the index specifically for the occurrence in core of a specific FA. It is defined as

$$\mathrm{NGI} = \left[\frac{(NT)_f}{(GT)_f}\right] \tag{1}$$

$(NT)_f$ and $(GT)_f$ are net and gross thicknesses, respectively, for the section of core and specific facies being considered. Hence, we refer to it as facies net-to-gross.

Sand Connectivity Index (SCI) SCI is an index that expresses the proportion of sand beds that are vertically connected in a representative TBT or VTBT FA. It is derived from the nature of bed or lamination cross-cutting relationships and forms an important discriminator for predicting sand vertical continuity and connectivity in a sequence of thin and very thin beds. It is expressed as a product of facies NGI (above) and a vertical connectivity factor (VCF). That is:

$$\mathrm{SCI} = [\mathrm{NGI}^*\mathrm{VCF}] \tag{2}$$

NGI is defined above, whereas VCF can be obtained as follows:

$$\mathrm{VCF} = \left[\frac{S/S}{((S/S) + (S/M))}\right] \tag{3}$$

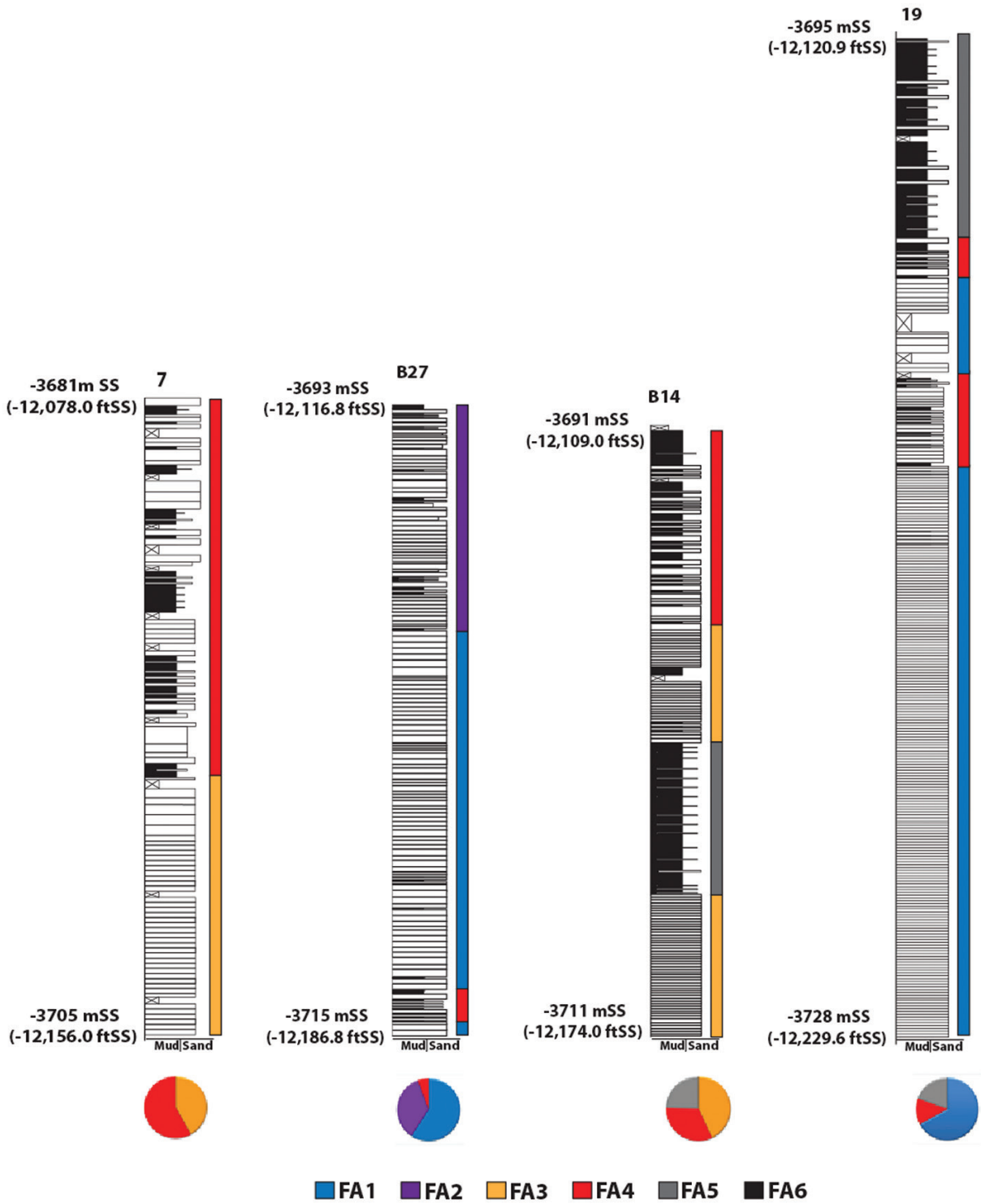

Figure 13. Simple lithology logs for wells 7, B27, B14, and 19, depicting proportion of each facies association identified in the wells. The proportions are plotted as pie charts. Location of sections within cored intervals are shown as blue thick lines in Figures 9A, 10A (the same intervals as in Figure 6); all are very close to the top of the Brae Formation.

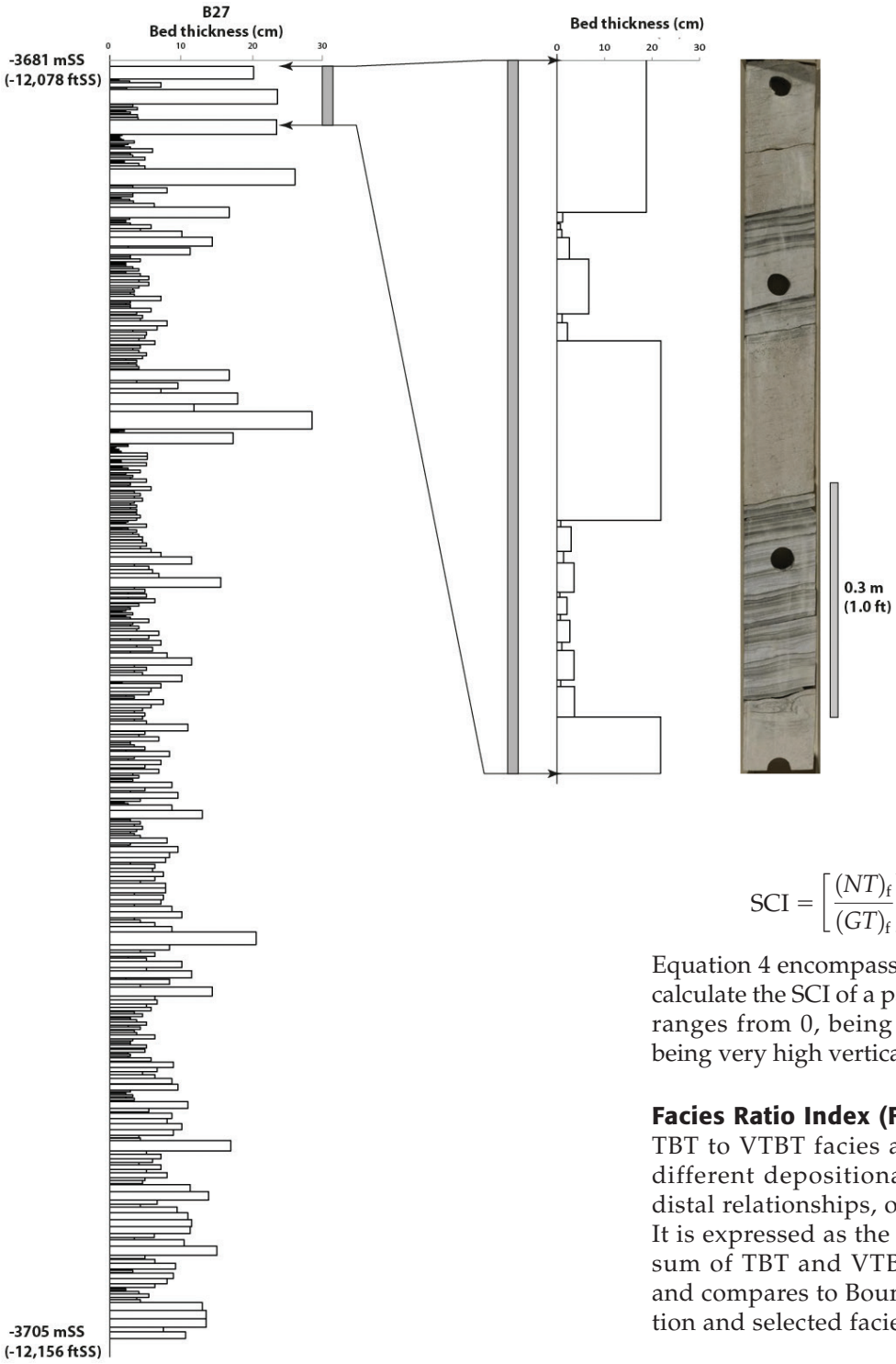

Figure 14. Left: A bed thickness profile across well B27 from −3681 to −3705 mSS (−12,078 to −12,156 ftSS). This is equivalent to 3984 to 4005 mMD (13,070–13,140 ftMD). Middle: Expanded section covering 3984 to 3985 mMD (13,070 to 13,073 ftMD). Right: Core photograph of the expanded section. In the context of our bed definition, the expanded section comprises 10 beds.

where S/S is the proportion of sand overlying sand and S/M is the proportion of sand overlying mud. So, the full SCI becomes

$$\mathrm{SCI} = \left[\frac{(NT)_f}{(GT)_f}\right] \times \left[\frac{S/S}{((S/S) + (S/M))}\right] \tag{4}$$

Equation 4 encompasses all variables that are used to calculate the SCI of a particular TBT and VTBT FA. SCI ranges from 0, being no vertical connectivity, to 1, being very high vertical connectivity.

Facies Ratio Index (FRI) FRI expresses the ratio of TBT to VTBT facies and is therefore distinctive of different depositional environments, proximal to distal relationships, or near-to-far channel location. It is expressed as the proportion of TBT beds to the sum of TBT and VTBT beds in a characteristic FA and compares to Bouma or Stow sequence combination and selected facies ratios. That is:

$$\mathrm{FRI} = \left[\frac{n\mathrm{TBT}}{\sum n(\mathrm{TBT};\ \mathrm{VTBT})}\right] \tag{5}$$

nTBT refers to number of TBT beds in a distinctive FA being considered, and $\sum n(\mathrm{TBT};\ \mathrm{VTBT})$ is the sum of TBT and VTBT in the FA. Like SCI, the FRI ranges

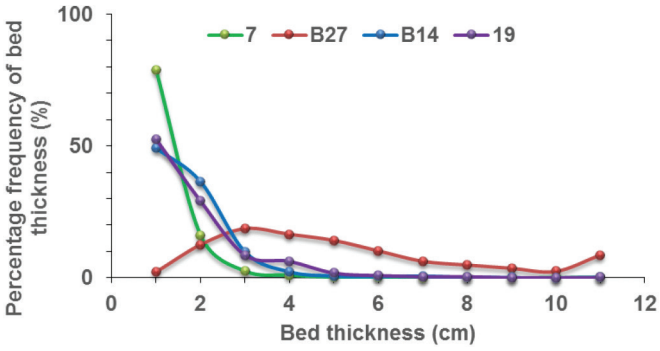

(A)

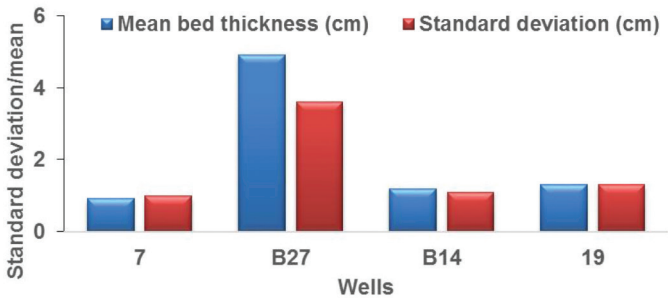

(B)

Figure 15. (Left) Statistical charts showing frequency of bed thickness (A) and mean bed thickness and standard deviation (B) within the cored intervals studied in detail. See text for explanation.

from 0 to 1 and it is indicative of the energy condition prevalent during sediment transport and subsequent deposition.

Sediment Textural Index (STI) STI is derived from the mean grain-size property of all the TBT–VTBT facies in the specific FA being considered. In particular, it is a measure of the difference in mean grain size between the coarser grained (sand-silt) beds and the finer grained (mud-rich) interbeds. It therefore considers the relative ease with which fluid can migrate through and be stored within the mudstone interbeds compared with the sandstone beds. It can provide insight into sediment transport, depositional history, and sediment maturity.

The STI is calculated by taking the reciprocal of mean grain size in ϕ units ($\bar{\delta}m$) of all the mud-rich interbeds minus the mean grain size in ϕ units ($\bar{\delta}s$) of all the sand-rich beds in the FA being considered. In each case, the nearest whole number ϕ unit is used. This is then multiplied by the NGI to account for the relative thickness of sandstone versus mudstone. This therefore becomes

$$\mathrm{STI} = \left(\frac{1}{(\bar{\delta}m - \bar{\delta}s)}\right) \times \mathrm{NGI} \qquad (6)$$

The STI ranges from 0 to 1, where values closer to 0 represent a large difference between sand and mud mean grain size and relatively thicker mudstone interbeds, whereas values closer to 1 represent a small difference between the sand and mud mean grain size and relatively thinner mudstone interbeds.

Attribute indices plots are presented in Figure 16A–C. The SCI, FRI, and STI are all plotted on the vertical axis against facies NGI. The values for each of the FAs are indicated by different colors. The axes are linear and values of respective attribute indices range from 0 to 1. In the cross plots, FAs 5 and 6 are not considered because of the extreme low values of their attribute indices arising from their mud-prone nature.

Different patterns are clearly observed for each of the four FAs considered. FA1 is marked by high-to-very-high NGI and SCI, a wide range of FRI, and a moderate-to-low STI. FA2 shows similar values but with greater spread of NGI and SCI and slightly lower values of FRI and STI. By contrast, FA4 has very-low-to-moderate NGI and very low SCI, FRI, and STI. FA3 shows a relatively greater spread of values for all indices that tend to span between the low values of FA4 and the high values of FA1 and FA2. Such plots can be used to derive average values for each attribute and for type facies, which can be used for input into reservoir modeling and simulation. They can also be used to consider attribute values that are more or less conducive to good reservoir properties and performance.

Porosity and Permeability

The results of porosity and permeability measurements are presented in Figures 17, 18 for well B27. FA1 samples have the highest porosity (21.8%), followed by FA2 with 13.5%. FA3 and FA4 have low porosity (10%) (Figure 17). During the permeability tests, only FA1 did permit appreciable flow of helium gas (Figure 18)—Kh, 998 md; Kv, 533 md (maximum); the other FAs did not permit gas flow despite their porosity (Omoniyi et al., 2015).

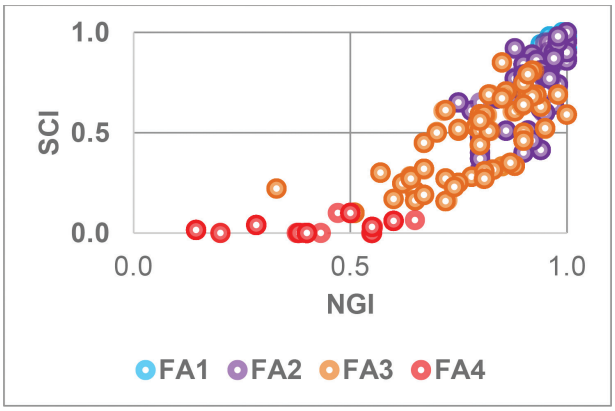

(A)

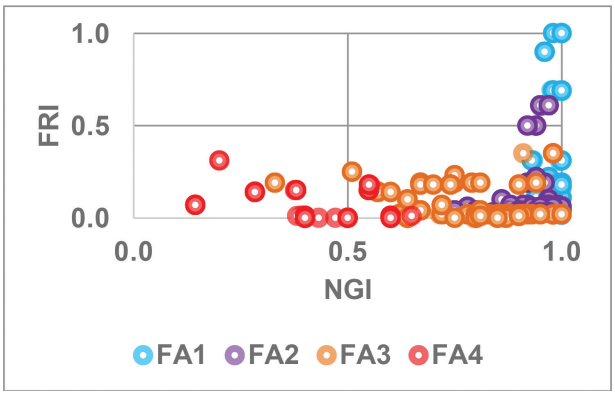

(B)

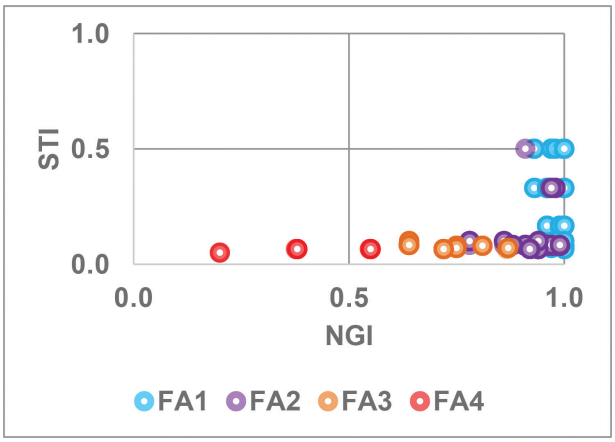

(C)

Figure 16. Cross plots for (A) SCI versus NGI, (B) FRI versus NGI, and (C) STI versus NGI for all facies associations in all the studied cores. The values for each of the facies associations are indicated by different colors. Many of the "individual" points are masking others with exactly the same values. The axes are linear and values of respective attribute indices range from 0 to 1. In the cross plots, facies associations 5 and 6 are not considered because of the extreme low values of their attribute indices arising from their mud-prone nature. See text for more explanation.

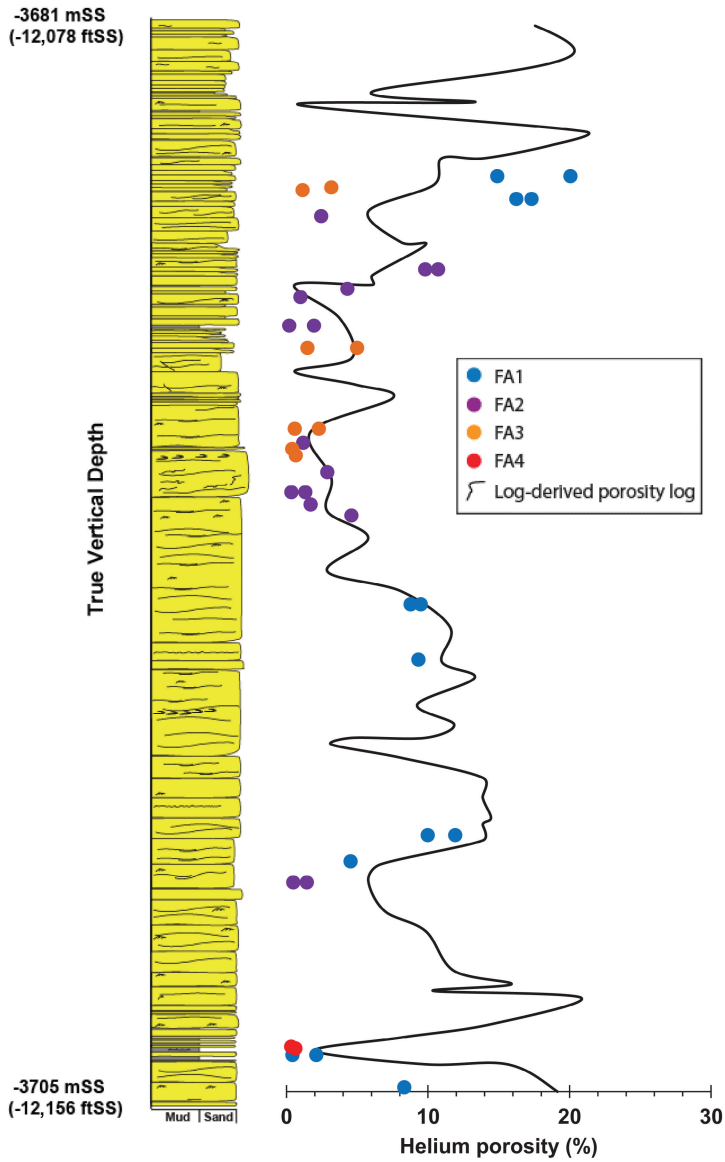

Figure 17. Wireline-derived porosity log correlated with ambient core-based porosity in well B27 (right). FA1 has the highest porosity and FA4 has the lowest. The low porosity values observed in some tight FA1 samples are caused by calcite cementation. The porosities are compared with the sedimentary log covering the cored interval in the well (left).

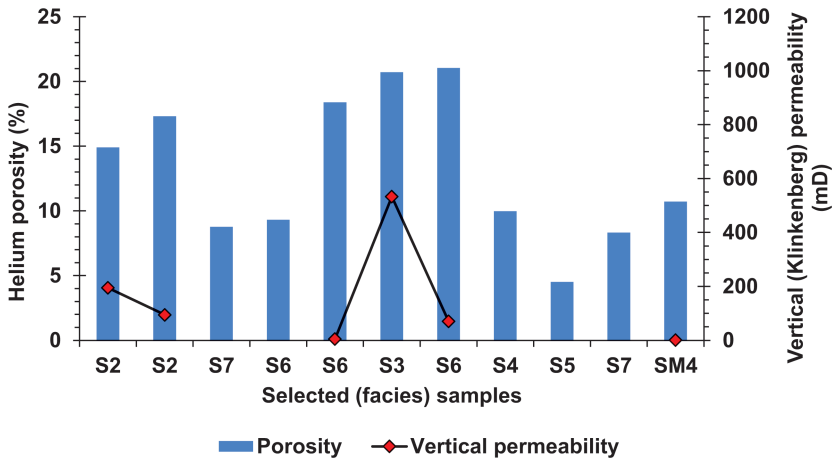

(A)

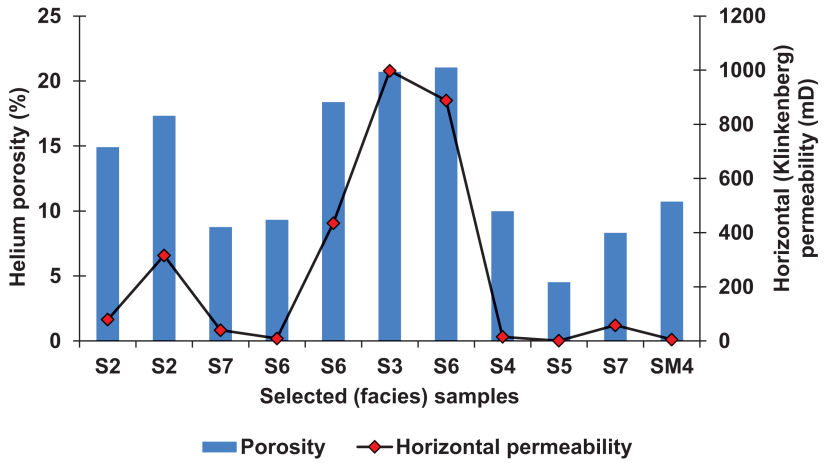

(B)

Figure 18. Representative figures showing distribution of porosity and vertical permeability (A), and porosity and horizontal permeability (B) in selected TBT facies samples. Only facies that belong to FA1 permitted appreciable gas (nitrogen) flow. More explanation is provided in the text.

DISCUSSION

Thin-bedded turbidites (both TBT and VTBT) have recently come under greater scrutiny from the industry to maximize return from deep-water investments and to optimize recovery from turbidite fields. From earlier work, it is clear that much still needs to be done in the characterization of TBT and VTBT, particularly in the context of quantifying their properties to permit prediction of sand geometry, sand quality, and sandstone/mudstone ratio, as well as to improve overall understanding of their distribution, architecture, and dynamic behavior. This is of paramount importance in reservoir modeling and simulation. The results presented in this study represent the first steps in developing a new approach to quantification of TBT and VTBT facies, which we have applied to the North Brae field in the North Sea.

Depositional Architecture

The wells studied in the North Brae field penetrate parts of a short-headed submarine fan that is part of a more extensive faulted slope-apron sedimentary system (Stow et al., 1982; Turner et al., 1987; Stephenson, 1991; Brehm, 2003). The system is fed by sediments sourced primarily from the Fladen Ground Spur in the west via a single input point (Fraser et al., 2003). Wells B8, B17, B1, and B7 were drilled through an elongated channel trending approximately west–east direction. Sand-matrix conglomeratic facies dominate in the proximal parts of the main conduit (thickest at well B1) and prograde eastward into predominantly sandstone facies of the mid-fan lobes. The thin-bedded sand-prone facies of well B27 is interpreted here as part of a sand-rich lobe lateral to the main channel system, and thicker sandstones in well B9 are interpreted

as more proximal parts of another lateral sand lobe (Figure 7; and see Turner et al., 2018). Adjacent to the main channel system on the northern flank, and in the proximal slope-apron adjacent to the input point conduit, turbidity-current deposition was dominated by mixed sandstone–mudstone (wells B14, 7, and 19) with both TBT and VTBT facies.

Synsedimentary tectonic activity has played a very significant role in both sediment supply and sediment architecture of the North Brae Fan. The style and response of TBT–VTBT facies to such tectonic activity is something that requires further investigation. Our first look at sequences of bed thickness reveals irregular, noncyclic patterns of thickness variation for most of the TBT–VTBT sections. There is some evidence for more distinctive small-scale oscillation sequences (or microcycles) in well B27. This may be characteristic of compensation cycles (Mutti and Sonnino, 1981; Piper and Stow, 1991) and especially typical of a lobe setting.

Facies, Attribute Indices, and Reservoir Character

Very careful logging and study of the TBT–VTBT succession in four selected wells led to the definition of 20 individual facies. These are grouped into six distinctive FAs, which can be more readily recognized and logged in future work. Careful development of a systematic method for characterizing these FAs in a rigorous and quantitative manner has led to the definition of four attribute indices used in this study: Facies NGI, SCI, FRI, and STI. Each index ranges in value from 0 to 1, where, for the most part, low values indicate more mud-prone facies and high values indicate sand-prone facies. However, these values do not necessarily correspond to poor or good reservoir characteristics. Cross plots between these indices allow us to determine relative properties of the different FAs and elucidate which are most suitable as potential reservoirs.

For good reservoir characteristics, we propose NGI > 0.7 and SCI > 0.7. FA1, FA2, and some FA3 match these criteria. The index level to set for FRI and STI is less clear-cut; a wider range of values appears to favor good reservoir characteristics. These indices should be used in conjunction with the other indices and are now the subject of further refinement and modification. Porosity–permeability measurements on core plugs closely matched the log-derived values. For porosity values, these measures concur with our evaluation of attribute indices. However, significant permeability measurement was only achieved for FA1, with lower values being obtained for FA2.

CONCLUSIONS

FA1 and FA2 have the best characteristics favorable for development in producing marginal turbidite fields with significant TBT–VTBT successions. This is related to their better porosity and permeability. In addition, they have high sandstone/mudstone ratio and the degree of heterogeneity is relatively low. These are followed by FA3, which can also be a good reservoir where NGI and SCI are both moderate to high. SCI is low in FA4, although sand percentage may be high, and as a result, this FA is unlikely to be a good reservoir. FA5 and FA6 are not considered suitable for conventional reservoir development. In general, the robust quantitative approach presented in this study could aid reservoir mapping, improve reservoir characterization of TBT and VTBT sequences, and could serve as input data for reservoir modeling of TBTs and VTBTs and associated deep-water elements. The practical applications of these indices for better prediction of sand continuity and connectivity and distribution of small-scale sedimentary heterogeneities are being explored and will be discussed elsewhere.

ACKNOWLEDGMENTS

This work was funded by TETFUND (Nigeria) and a Watt Scholarship (HWU). We thank Marathon Oil Company for supplying the cores, and the British Geological Survey, Keyworth, for access to the National Core Repository. We warmly thank Colin Turner and Bryan Cronin for their comments on the manuscript, Sally Hamilton for her technical support, and the reviewers for their instructive feedback.

REFERENCES

Branter, S., 2003, The East Brae Field, Blocks 16/03a, 16/03b, UK North Sea, *in* J. G. Gluyas and H. M. Hichens, eds., United Kingdom oil and gas fields: Commemorative millennium volume: Geological Society (London) Memoir 20, p. 191–197.

Brehm, J. A., 2003, The North Brae and Beinn Fields, Block 16/7a, UK North Sea, *in* J. G. Gluyas and H. M. Hichens, eds., United Kingdom oil and gas fields: Commemorative millennium volume: Geological Society (London) Memoir 20, p. 199–209.

Browne, G. H., and R. M. Slatt, 2002, Outcrop and behind-outcrop characterization of a late Miocene slope fan system, Mt. Messenger Formation, New Zealand: AAPG Bulletin, v. 86, p. 841–862.

Clemenceau, G. R., 1995, Ram/Powell Field: Viosca Knoll Block 912, deepwater Gulf of Mexico, *in* R. D. Winn and J. M. Armentrout, eds., Turbidites and associated deepwater facies: SEPM Core Workshop 20, p. 95–129.

Clemenceau, G. R., J. Colbert, and D. Edens, 2000, Production results from levee-overbank turbidite sands at Ram/Powell Field, deepwater Gulf of Mexico, *in* P. Weimer, ed., Deep-water reservoirs of the world: SEPM 20th Annual Research Conference, Houston Texas, December 3–6, 2000, p. 241–251.

Fletcher, K. J., 2003, The Central Brae Field, Blocks 16/07a, 16/07b, UK North Sea, *in* J. G. Gluyas and H. M. Hichens, eds., United Kingdom oil and gas fields: Commemorative millennium volume: Geological Society (London) Memoir 20, p. 183–190.

Fraser, S., A. Robinson, H. Johnson, J. Underhill, and D. Kadolsky, 2003, Upper Jurassic, *in* D. Evans, C. Graham, A. Armour, and P. Bathurst, eds., The millennium atlas: Petroleum geology of the central and northern North Sea: Geological Society (London), p. 157–189.

Garland, C. R., 1993, Miller Field: Reservoir stratigraphy and its impact on development, *in* J. R. Parker, ed., Petroleum geology of northwest Europe: Proceedings of the 4th Conference: Geological Society (London), p. 401–414.

Gill, C. E., and M. Shepherd, 2010, Locating the remaining oil in the Nelson Field, *in* B. A. Vining and S. C. Pickering, eds., Petroleum geology: From mature basins to new frontiers: Proceedings of the 7th Petroleum Geology Conference: Geological Society (London), p. 349–368.

Gluyas, J. G., and S. W. Garrett, 2005, Better recovery through better reservoir characterization: Overview, *in* A. G. Dore and B. A. Vining, eds., Petroleum geology of north-west Europe and global perspectives: Proceedings of the 6th Petroleum Geology Conference: Geological Society (London), p. 361–365.

Harms, J. C., P. Tackenberg, E. Pickles, and R. E. Pollock, 1981, The Brae Oilfield Area, *in* L.V. Illing and G.D. Hobson, eds., Petroleum geology of the continental shelf of north-west Europe: London, Institute of Petroleum, p. 352–357.

Hempton, M., J. Marshall, S. Sadler, N. Hogg, R. Charles, and C. Harvey, 2005, Turbidite reservoirs of the Sele Formation, Central North Sea: Geological challenges for improving production, *in* A. G. Dore and B. A. Vining, eds., Petroleum geology of north-west Europe and global perspectives: Proceedings of the 6th Petroleum Geology Conference: Geological Society (London), p. 449–459.

Hurst, A., A. J. Fraser, S. I. Fraser, and F. Hadler-Jacobsen, 2005, Deep-water clastic reservoirs: A leading global play in terms of reserve replacement and technological challenges, *in* A. G. Dore and B. A. Vining, eds., Petroleum geology of north-west Europe and global perspectives: Proceedings of the 6th Petroleum Geology Conference, Geological Society (London), p. 1111–1120.

Khain, V. E., and I. D. Polyakova, 2004, Oil and gas potential of deep- and ultra deep-water zones of continental margins: Lithology and mineral resources, v. 39, p. 530–540.

Lerch, C. S., K. W. Bramlett, W. H. Butler, J. N. Scales, T. B. Stroud, and C. A. Glandt, 1996, Integrated 3D reservoir modeling at Ram-Powell field: A turbidite reservoir in the eastern Gulf of Mexico: SPE Annual Technical Conference and Exhibition, Denver, October 6–9, 1996, p. 477–492.

Mutti, E., and M. Sonnino, 1981, Compensation cycles: A diagnostic feature of turbidite sandstone lobes: 2nd European Regional Meeting of International Association of Sedimentologists, p. 120–123.

Newton, S. K., and K. P. Flanagan, 1993, The Alba Field: Evolution of the depositional model, *in* J. R. Parker, ed., Petroleum geology of northwest Europe: Proceedings of the 4th Conference, Geological Society (London), p. 161–171.

Omoniyi, B. A., D. A. V. Stow, and A. Gardiner, 2014, Characterisation of thin-bedded turbidites for field value optimisation, *in* C. C. Turner and B. T. Cronin, eds., The 'Brae Play', South Viking Graben; Jurassic coarse-grained clastic reservoirs, structural development and hydrocarbon systems: Conference Abstracts, Aberdeen, Scotland, 23–24 April 2014, p. 54.

Omoniyi, B. A., D. A. V. Stow, and A. Gardiner, 2015, Quantitative assessment of reservoir quality in thin-bedded turbidite facies: 31st IAS Meeting of Sedimentology, Conference Abstracts, Krakow, Poland, June 22–25, 2015, p. 506.

Pettingill, H. S., 1998, Lessons learned from 43 turbidite giant fields: Oil and Gas, v. 96, p. 93–95.

Piper, D. J. W., and D. A. V. Stow, 1991, Fine-grained turbidites, *in* G. Einsele, W. Ricken, and A. Seilacher, eds., Cycles and events in stratigraphy: Berlin, Springer-Verlag, p. 360–376.

Richards, P. C., G. K. Lott, H. Johnson, R. W. O. B. Knox, and J. B. Riding, 1993, Jurassic of the central and northern North Sea, *in* R. W. O. B. Knox and W. G. Cordey, eds., Lithostratigraphic nomenclature of the UK North Sea: UKOOA Lithostratigraphic Nomenclature 3, p. 219.

Roberts, M. J., 1991, The South Brae Field, Block 16/7a, UK North Sea, *in* I. L. Abbotts, ed., United Kingdom oil and gas fields: 25 years commemorative volume: Geological Society (London) Memoir 14, p. 55–62.

Rooksby, S. K., 1991, The Miller Field, Blocks 16/7b, 16/8b, UK North Sea, *in* I. L. Abbotts, ed., United Kingdom oil and gas fields: 25 years commemorative volume: Geological Society (London) Memoir 14, p. 159–164.

Selley, R. C., 2000, Applied sedimentology: Orlando, Academic Press, 523 p.

Shepherd, M., 1991, The Magnus Field, Blocks 211/7a, 12a, UK North Sea, *in* I. L. Abbotts, ed., United Kingdom oil and gas fields: 25 years commemorative volume: Geological Society (London) Memoir 14, p. 153–157.

Spence, S., and H. Kreutz, 2003, The Kingfisher Field, Block 16/8a, UK North Sea, *in* J. G. Gluyas and H. M. Hichens, eds., United Kingdom oil and gas fields: Commemorative millennium volume: Geological Society (London) Memoir 20, p. 305–314.

Stephenson, M. A., 1991, The North Brae Field, Block 16/7a, UK North Sea, *in* I. L. Abbotts, ed., United Kingdom oil and gas fields: 25 years commemorative volume: Geological Society (London) Memoir 14, p. 43–48.

Stow, D. A. V., 1984, Upper Jurassic overlapping-fans slope-apron system: Brae oilfield, North Sea: Geo-Marine Letters, v. 3, p. 217–222.

Stow, D. A. V., 2000, Thin-bedded turbidites and associated facies: Their nature, geometry and reservoir properties, *in* C. J. Appi, ed., Deep-water sedimentation: Technological challenges for the next millennium: Rio de Janeiro, Brazilian Association of Petroleum Geologists, p. 40–41.

Stow, D. A. V., 2005, Sedimentary rocks in the field, a colour guide: London, Manson Publishing, 320 p.

Stow, D. A. V., C. D. Bishop, and S. J. Mills, 1982, Sedimentology of the Brae oilfield, North Sea: Fan models and controls: Petroleum Geology, v. 5, p. 19.

Stow, D. A. V., A. Gardiner, G. Pickup, and U. Patel, 2012, Geological attributes of fine-grained turbidites as unconventional reservoirs: SPE/EAGE European Unconventional Resources Conference and Exhibition, Vienna, Austria, March 20–22, 2012 (abs.).

Stow, D. A. V., D. G. Howell, and C. H. Nelson, 1983, Sedimentary, tectonic, and sea-level controls on submarine fan and slope-apron turbidite systems: Geo-Marine Letters, v. 3, p. 57–64.

Stow, D. A. V., and M. Mayall, 2000, Deep-water sedimentary systems: New models for the 21st century: Marine and Petroleum Geology, v. 17, p. 125–135.

Stow, D. A. V., H. G. Reading, and J. D. Collinson, 1996, Deep seas, *in* H. G. Reading, ed., Sedimentary environments: Processes, facies, and stratigraphy: Oxford, Blackwell Science, p. 395–453.

Turner, C. C., and P. J. Allen, 1991, The Central Brae Field, Block 16/7a, UK North Sea, *in* I. L. Abbotts, ed., United Kingdom oil and gas fields: 25 years commemorative volume: Geological Society (London) Memoir 14, p. 49–54.

Turner, C. C., Bastidas, R. E., Connell, E. R., and Petrik, F. E., 2018, Proximal submarine fan reservoir architecture and development in the Upper Jurassic Brae Formation of the Brae Fields, South Viking Graben, U.K North Sea, *in* C. C. Turner and B. T. Cronin, eds., Rift-related coarse-grained submarine fan reservoirs; the Brae Play, South Viking Graben, North Sea: AAPG Memoir 115, p. 213–256.

Turner, C. C., J. M. Cohen, E. R. Connell, and D. M. Cooper, 1987, A depositional model for the South Brae oilfield, *in* J. Brooks and K. W. Glennie, eds., Petroleum geology of north-west Europe: London, Graham & Trotman, p. 853–864.

Turner, C. C., and E. R. Connell, 1991, Stratigraphic relationships between Upper Jurassic submarine fan sequences in the Brae area, UK North Sea: The implications for reservoir distribution: Offshore Technology Conference, Houston, Texas, May 6–9, 1991, p. 83–91.

Worthington, P. F., 2010, A road map for the identification and recovery of by-passed pay, *in* B. A. Vining and S. C. Pickering, eds., Petroleum Geology Conference Series: Geological Society (London) Conference Series 7, p. 453–462.

Wright, S., 2003, The West Brae and Sedgwick Fields, Blocks 16/06a, 16/07a, UK North Sea, *in* J. G. Gluyas and H. M. Hichens, eds., United Kingdom oil and gas fields: Commemorative millennium volume: Geological Society (London) Memoir 20, p. 223–231.